ISSN 0972-0405

ISET JOURNAL OF EARTHQUAKE TECHNOLOGY

Vol. 47 No. 2-4 June-Dec. 2010

CONTENTS

Financial Assistance from AICTE and DST, New Delhi for the Publication of ISET Journals for 2010–2011 is duly acknowledged.

ISET Journal of Earthquake Technology, Paper No. 510, Vol. 47, No. 2-4, June-Dec. 2010, pp. 61–74

IMPORTANCE OF SITE-SPECIFIC STUDIES FOR MEDIUM SOIL SITES OF DELHI REGION

P. Kamatchi*, G.V. Ramana** and A.K. Nagpal**
*Structural Engineering Research Centre, CSIR Campus, Taramani, Chennai-600113
**Department of Civil Engineering, IIT Delhi, Hauz Khas, New Delhi-110016

ABSTRACT

The importance of the effects of sediments above bedrock in modifying the strong ground motion has been long recognized. To account for this, some codes of practice incorporate individual response spectra for different types of soil. As an improvement over this, the amplification factors derived out of empirical and theoretical data are suggested in some of the international seismic codes for different site classes. In these codes, site-specific analysis has been recommended for the soft soil type (i.e., Site Class F). In this paper, the importance of site-specific response for three actual medium soil sites of Delhi is investigated. For this the scenario earthquakes from the Himalayan region as reported in the literature are chosen. It is demonstrated that for the Delhi region it may be necessary to perform site-specific analyses also for the buildings at the sites having medium types of soil.

KEYWORDS: Site-Specific Analysis, Delhi, Strong Ground Motion Generation, Soil Amplification

INTRODUCTION

The importance of the effects of sediments above bedrock in modifying a strong ground motion has been long recognized (Boore, 2004; Boore and Joyner; 1997; Idriss and Seed, 1970; Seed and Idriss, 1969; Lam et al., 2001; Govindarajulu et al., 2004) in the literature. The nature of soil that changes the amplitude and frequency content of a ground motion has a major influence on the damaging effects of an earthquake. To account for these effects, most of the seismic codes, for example the Indian code (BIS, 2002), have defined response spectra for three types of soil, viz., hard soil, medium soil and soft soil. As an improvement over this approach, amplification factors based on empirical and theoretical data (Borcherdt, 1994) have been introduced in the International Building Code (ICC, 2000) for the site classes A to F, in the short-period and long-period ranges, based on the average shear wave velocity of the top 30 m soil stratum. It has been recommended that for the site class F (i.e., soft soil), additional site-specific studies be carried out. It has been also recommended (Heuze et al., 2004) that in addition to the use of seismic code provisions, analyses for the scenario earthquakes be carried out.

For the Delhi region, seismologists (Bilham et al., 1998; Singh et al., 2002) have reported that three major thrust planes, viz., Main Central Thrust (MCT), Main Boundary Thrust (MBT), and Main Frontal Thrust (MFT) exist in Himalayas due to the relative movement of Indian plate by 5 cm/year with respect to the Eurasian plate. Khattri (1999) has estimated the probability of occurrence of a great earthquake of 8.5 moment magnitude from the large unbroken segment called central seismic gap (see Figure 1) between MBT and MCT in the next 100 years to be 0.59. Delhi is situated at a distance of roughly 200 km from MBT and 300 km from MCT.

In this paper, site-specific studies have been carried out for three actual sites (of medium soil) at Delhi for which borelog details are available up to the rock. Rock outcropping motions have been generated for a reference site at the Delhi Ridge observatory, for the scenario earthquakes of moment magnitude M_w = 7.5, 8.0 and 8.5 from central seismic gap of Himalayan region.

STRONG MOTION GENERATION

Recorded ground motions are not available for the Delhi region. Hence, in the present study artificial strong motions are generated using a stochastic model. Ground motions are generated by identifying the major fault zones and propagating seismic waves generated at these potential sources to the sites of interest. Path effects and anelastic attenuation effects are well predicted by the empirical and theoretical models (Beresnev and Atkinson, 2002). For source representation, point source models (Boore and Atkinson, 1987) or finite source models (Hartzell, 1978) are widely used.

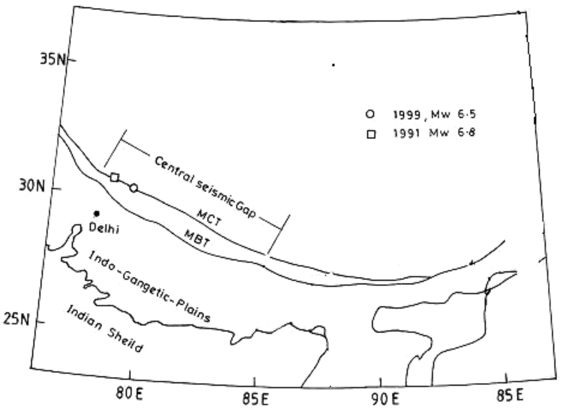

Fig. 1 Central seismic gap of Himalayan region

The stochastic simulation procedure for ground motion generation based on seismological models using point source model has been proposed by Boore (1983, 2003). In this procedure a band-limited Gaussian white noise is windowed and filtered in time domain and transformed into frequency domain. The Fourier amplitude spectrum is scaled to the mean-squared absolute spectra and multiplied by a Fourier amplitude spectrum obtained from the source path effects. Then, the spectrum is transformed back to time domain and the desired time history is obtained.

From the analysis of recorded ground motions, it has been reported (Beresnev and Atkinson, 1997) that point source models are not capable of reproducing the characteristic features of large earthquakes (i.e., M_w > 6), viz., long durations and radiation of less energy at low-to-intermediate frequencies (i.e., 0.2–2 Hz). The simulation of strong ground motions from finite fault rupture has been developed by Beresnev and Atkinson (1997, 1998). The fault rupture plane is modeled with an array of sub-faults and the radiation from each sub-fault is modeled as a point source similar to the model of Boore (1983). According to the finite source model, fault rupture initiates at the hypocenter and spreads uniformly along the fault plane radially outward with a constant rupture velocity, thus triggering radiations from the sub-faults in succession.

The Fourier amplitude spectrum $A(\omega)$ of the point source of one element (or sub-fault) is defined as (Boore, 1983; Boore and Atkinson, 1987; Brune, 1970)

$$A(\omega) = \omega^2 S(\omega) P(\omega) G(R) A_n(\omega) \tag{1}$$

where ω is the angular frequency, $S(\omega)$ is the source function, $P(\omega)$ is the filter function for high-frequency attenuation, $G(R)$ is the geometric attenuation function, and $A_n(\omega)$ is the anelastic whole path attenuation function. These functions are further defined below.

1. Source Function, $S(\omega)$

The shape and amplitude of the theoretical source spectrum (i.e., ω^2-model) given by Aki (1967)) is as follows:

$$S(\omega) = \frac{PFR^{\theta\varphi} m_o}{4\pi\rho\beta^3 r} \frac{1}{\left[1+\left(\omega/\omega_c\right)^2\right]} \tag{2}$$

where P is the partition factor to represent one horizontal component, F is the free-surface amplification factor, $R^{\theta\varphi}$ is the spectral average for radiation pattern, m_o is the seismic moment of a sub-fault, ω_c is the corner frequency, ρ is the density in the vicinity of the source in g/cm^3, β is the shear wave velocity in km/s, and r is the distance in km from the point source to the point of observation, within which the intervening medium is assumed to be homogeneous and non-absorbing. In the simulation of ground motion for the Delhi region in the present study, the values of different parameters are adopted (Singh et al., 2002) as $P = 1/\sqrt{2}$, $F = 2.0$, $R^{\theta\varphi} = 0.55$, $\rho = 2.85$ gm/cc, $r = 1.0$ km, and $\beta = 3.6$ km/s.

The moment magnitude M_w which defines the size of earthquake, is related (Hanks and Kanamori, 1979) to the seismic moment M_0 of the earthquake as

$$M_w = 0.67 \log M_0 - 10.7 \tag{3}$$

The rupture area A and sub-fault length Δl corresponding to the moment magnitude of earthquake can be calculated from the empirical equations (Beresnev and Atkinson, 1998) as follows:

$$\log A = M_w - 4.0 \tag{4}$$

$$\log \Delta l = -2 + 0.4\, M_w \tag{5}$$

For a sub-fault of equal dimensions ($\Delta w = \Delta l$, with Δw and Δl being the dimensions of the sub-fault), the seismic moment m_0 of the sub-fault is given by

$$m_0 = \Delta\sigma \left(\Delta l\right)^3 \tag{6}$$

where $\Delta\sigma$ is the stress parameter (Beresnev and Atkinson, 1998). The number of sub-sources, N_{sub}, to be summed to reach the target seismic moment (i.e., M_0) is given by

$$N_{\text{sub}} = \frac{M_0}{m_0} \tag{7}$$

The corner frequency ω_c that governs the acceleration amplitude and controls the frequency content of the earthquake at source is given by

$$\omega_c = \frac{2 y_r z_s \beta}{\Delta l} \tag{8}$$

where y_r is the constant representing the ratio of rupture velocity to the shear wave velocity of source, and z_s is the parameter indicating the maximum rate of slip, also known as strength factor. The value of y_r is set equal to 0.8 by Beresnev and Atkinson (1997). The value of z_s may vary from 0.5 to 2.0, and in the present study a value of 1.4 (Singh et al., 2002) has been adopted for the simulation of earthquake motions for the Delhi region.

2. Filter Function for High-Frequency Attenuation, $P(\omega)$

In order to account for high-frequency attenuation by the near-surface weathered layer, either a fourth-order Butterworth filter with the cut-off frequency $\omega_m = 2\pi f_{\max}$ or a spectral decay parameter κ is widely used in stochastic models. In the present study, the Butterworth filter function $P(\omega)$ with the cut-off frequency $f_{\max} = 15$ Hz (Singh et al., 2002) is adopted:

$$P(\omega) = \left[1 + \left(\omega/\omega_m\right)^8\right]^{-1/2} \tag{9}$$

3. Geometric Attenuation Factor, $G(R)$

Geometric attenuation accounts for the decay and type of seismic waves. According to Singh et al. (2002) and Herrmann and Kijko (1983), for a distance of twice the crustal thickness body waves dominate (the direct seismic shear waves) and after that surface waves dominate (the reflected L_g waves). Depending on the thickness of earth's crust, trilinear or bilinear relationships are used for the calculation of $G(R)$. The thickness of crust near Delhi has been reported to be 45–50 km (Tewari and Kumar (2003)) and hence following bilinear relationship is adopted in the present study:

$$G(R) = \frac{1}{R} \qquad R < 100 \text{ km} \tag{10a}$$

$$G(R) = \frac{1}{\sqrt{100R}} \qquad R > 100 \text{ km} \tag{10b}$$

4. Anelastic Whole Path Attenuation Factor, $A_n(\omega)$

The anelastic whole path attenuation factor $A_n(\omega)$ which represents wave energy loss due to the radiation damping of rocks is expressed as

$$A_n(\omega) = e^{-\omega R / 2Q\beta} \tag{11}$$

where Q is the quality factor. The Q factor depends on the wave transmission quality of rocks. For the Himalayan arc region, the Q factor has been estimated by Singh et al. (2002) from the available earthquake records as

$$Q(f) = 508 f^{0.48} \tag{12}$$

where f is the frequency in Hz.

5. Simulation of Time History

The Fourier amplitude spectrum derived above gives the frequency content of the earthquake ground motion. This frequency information is combined with random phase angles in a stochastic process to generate artificial ground motion (Boore, 1983) for each sub-fault. Simulations from all sub-faults are then lagged and summed to get the time history of earthquake.

The duration of the sub-fault time window, T_w, is represented as the sum of its source duration, T_s, and distance-dependant duration, T_d (Beresnev and Atkinson, 1997; Boore, 2003):

$$T_w = T_s + T_d \tag{13}$$

Further, T_s is taken as proportional to the inverse of the corner frequency (i.e., $1/f_c$) and T_d is taken as $0.05R$ (Beresnev and Atkinson, 1997; Boore, 2003).

The finite fault simulation program (FINSIM) has been widely used for the generation of ground motions of large-size earthquakes (Atkinson and Beresnev, 2002; Beresnev and Atkinson, 1998; Roumelioti and Beresnev, 2003; Singh et al., 2002) and hence has been adopted in the present study.

ONE-DIMENSIONAL WAVE PROPAGATION: EQUIVALENT LINEAR ANALYSIS

The one-dimensional, equivalent linear, vertical wave propagation analysis is the widely used numerical procedure for modeling the soil amplification problems (Idriss, 1990; Yoshida et al., 2002). The equivalent linear analysis program SHAKE (Ordóñez, 2002; Schnabel et al., 1972) has been used in the present study. Since SHAKE is a total stress analysis program (Schnabel et al., 1972), the depth of water table has not been considered in the analysis.

TYPICAL SOIL STRATA FOR DELHI REGION

Three actual soil sites in Delhi, designated as Site 1, Site 2 and Site 3 (see Figure 2), are chosen for studying the building response. The layerwise soil characteristics (of the medium type soil) and the depth to the base of each layer from the surface are given in Tables 1–3.

The measurements of shear wave velocity V_s are not available for the sites chosen. However, the variations of N values with depth are available from the geotechnical data (see Tables 1–3). The variation of shear wave velocity with depth for the present study is obtained by using the correlations suggested for the Delhi region by Rao and Ramana (2004):

$$V_s = 79 N^{0.43} \text{ for sand} \tag{14a}$$

$$V_s = 86N^{0.42} \text{ for sandy silt/silty sand} \quad (14b)$$

The modulus reduction $G/G_{\max}$ and damping ratio ζ curves are adopted from Vucetic and Dobry (1991), depending on the plasticity index of the soil stratum.

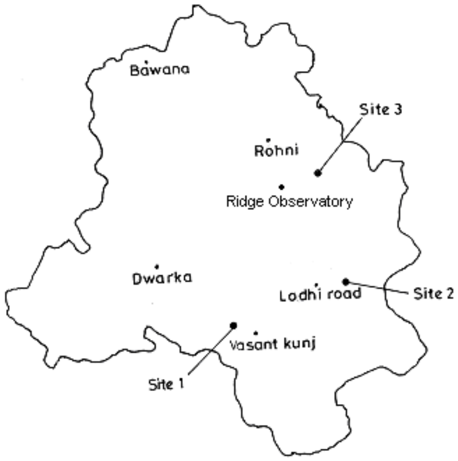

Fig. 2 Three typical soil sites in Delhi

Table 1: Geotechnical Profile at Site 1

Layer No.	Description	Thickness (m)	Depth to the Bottom of Layer (m)	SPT (N Value)	Shear Wave Velocity V_s (m/s)	Plasticity Index (%)	Total Unit Weight (kN/m^3)
1	Sandy Silt of Low Plasticity	3.5	3.5	13	252.55	7	16.3
2		1.5	5	17	282.67		
3		1.5	6.5	20	302.64		
4		1.5	8	23	320.94		
5	Sandy Silt of Low Plasticity	1.5	9.5	28	348.58	7	16.9
6		1.5	11	32	368.69		
7		1.5	12.5	35	382.83		
8		1.5	14	37	391.87	6	18.1
9		1.5	15.5	42	413.30		18.5
10		1.5	17	47	433.29		18.5
11	Rock	—		—	1500	—	24.0

Table 2: Geotechnical Profile at Site 2

Layer No.	Description	Thickness (m)	Depth to the Bottom of Layer (m)	SPT (N Value)	Shear Wave Velocity V_s (m/s)	Plasticity Index (%)	Total Unit Weight (kN/m^3)
1	Clayey Silt of Low Plasticity	1.5	1.5	9	216.41	11	16.9
2		1.5	3.0	9	216.41	15	17.4
3	Sandy Silt	1.5	4.5	12	229.97	Non Plastic	17.4
4	Fine Sand	1.5	6.0	12	229.97		17.2
5		1.5	7.5	12	229.97		17.1
6		1.5	9.0	13	238.03		17.1

7		1.5	10.5	15	253.13		17.1
8		1.5	12.0	19	280.21		17.1
9		1.5	13.5	20	286.46		17.7
10		1.5	15.0	21	292.54		17.7
11		1.5	16.5	26	320.68		17.7
12	Sandy Silt of Low Plasticity	1.5	18.0	31	363.81		17.7
13		1.5	19.5	41	409.14		17.7
14		1.5	21.0	41	409.14	6	19.8
15		1.5	22.5	41	409.14		19.8
16	Rock	-		-	1500	-	24.0

Table 3: Geotechnical Profile at Site 3

Layer No.	Description	Thickness (m)	Depth to the Bottom of Layer (m)	SPT (N Value)	Shear Wave Velocity V_s (m/s)	Plasticity Index (%)	Total Unit Weight (kN/m^3)
1	Sandy Silt	3.5	3.5	5	169.07	Non Plastic	16.3
2		1.5	5.0	6	182.52		16.3
3		1.5	6.5	7	194.73		16.3
4		1.5	8.0	9	216.41		17.1
5		1.5	9.5	11	235.44		17.1
6		1.5	11.0	14	260.54		17.1
7		1.5	12.5	13	252.55		17.4
8		1.5	14.0	27	343.30		17.4
9	Clayey Silt	1.5	15.5	36	387.39	15	17.7
10		1.5	17.0	32	368.69	15	17.7
11		1.5	18.5	13	252.55	15	17.7
12		1.5	20.0	28	348.58	15	17.7
13	Sandy Silt	1.5	21.5	45	425.45	Non Plastic	18.1
14		1.5	23.0	28	348.58		18.1
15		1.5	24.5	42	413.30		18.1
16		1.5	26.0	44	421.45		18.5
17		1.5	27.5	47	433.29		18.5
18		1.5	29.0	> 50	444.70		18.5
19		1.5	30.5		444.70		19.8
20		1.5	32.0		444.70		19.8
21		1.5	33.5		444.70		19.8
22		1.5	35.0		444.70		19.8
23		1.5	36.5		444.70		19.8
24		1.5	38.0		444.70		19.8
25	Rock	-			1500	-	24.0

RESPONSE OF THREE SITES FOR SCENARIO EARTHQUAKES

The seismological parameters (see Table 4) used in the generation of rock outcrop motions for the Delhi region are broadly adopted from Singh et al. (2002). In order to minimize the noise due to random fault rupture in the simulation, 15 ground motions have been generated for each earthquake magnitude. One of these simulations of the time histories for rock outcrop (at Ridge Observatory) is compared (see Figure 3) with a simulation obtained by S.K. Singh (personal communication), for each of the magnitudes 7.5, 8.0 and 8.5.

Table 4: Seismological Parameters for Strong-Motion Generation

Parameters	M_w **= 7.5**	M_w **= 8.0**	M_w **= 8.5**
Fault orientation	Strike 300° Dip 7°	Strike 300° Dip 7°	Strike 300° Dip 7°
Fault dimension along strike and dip (km)	56×56	125×80	240×80
Depth of focus (km)	11	16	16
Stress parameter (bar)	50	50	50
No. of sub-faults	5×5	8×5	16×5
No. of sub-sources summed	28	57	339
Duration model	$1/f_c + 0.05R$	$1/f_c + 0.05R$	$1/f_c + 0.05R$
Quality factor	$508\,f^{0.48}$	$508\,f^{0.48}$	$508\,f^{0.48}$
Windowing function	Saragoni-Hart	Saragoni-Hart	Saragoni-Hart
$f_{\max}$ (Hz)	15	15	15
Crustal shear wave velocity (km/s)	3.6	3.6	3.6
Crustal density (kN/m^3)	2.8	2.8	2.8
Radiation strength factor	1.4	1.4	1.4

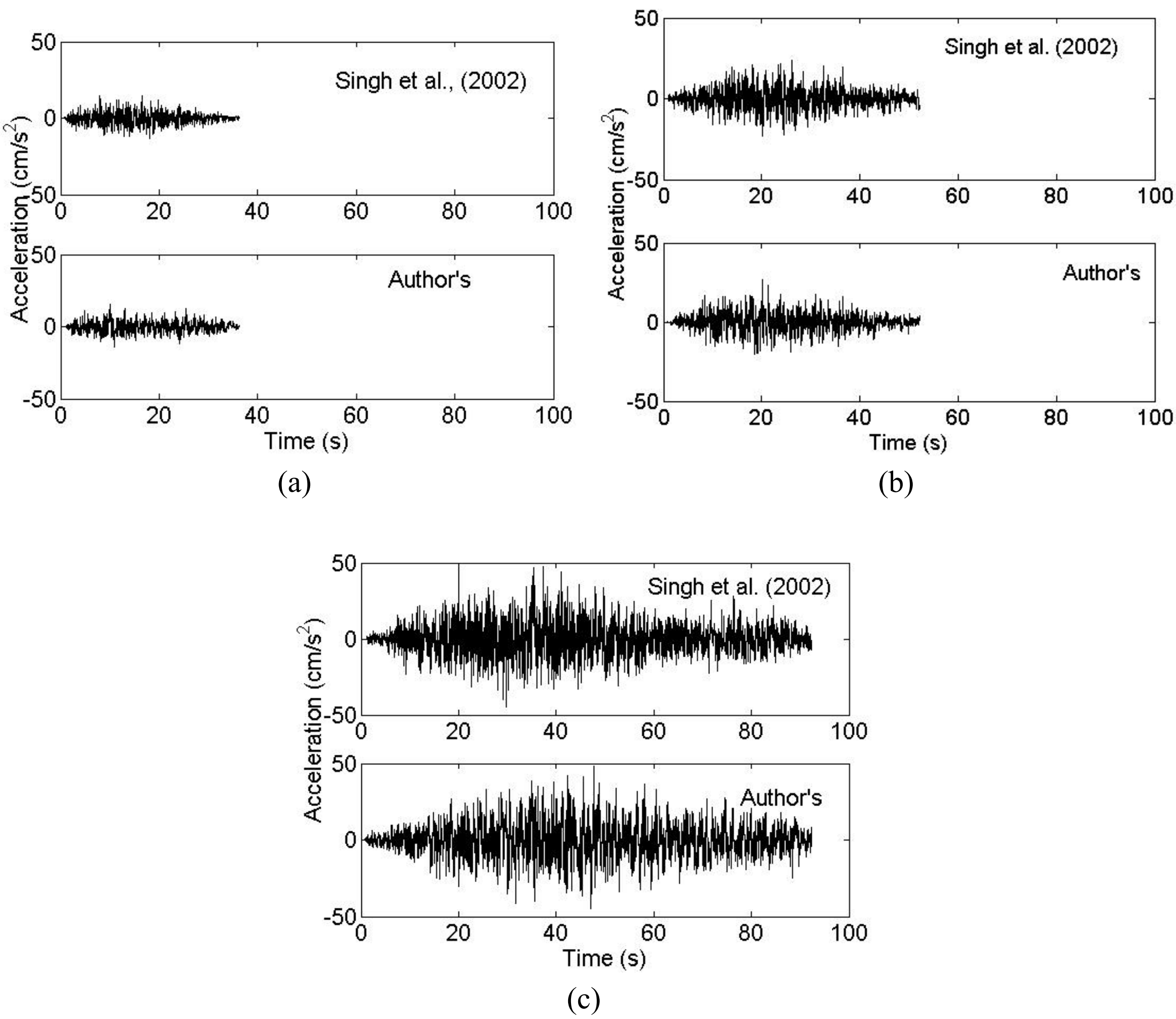

Fig. 3 Comparisons of the simulations of rock outcrop motions from present study and Singh et al. (2002): (a) M_w = 7.5; (b) M_w = 8.0; and (c) M_w = 8.5

The rock outcrop motions simulated above are propagated through the soil strata of the three sites and the free-field motions are obtained. As a typical case, the bedrock level and free-field motions at the top of the three sites for one simulation in the case of M_w = 7.5 are shown in Figure 4.

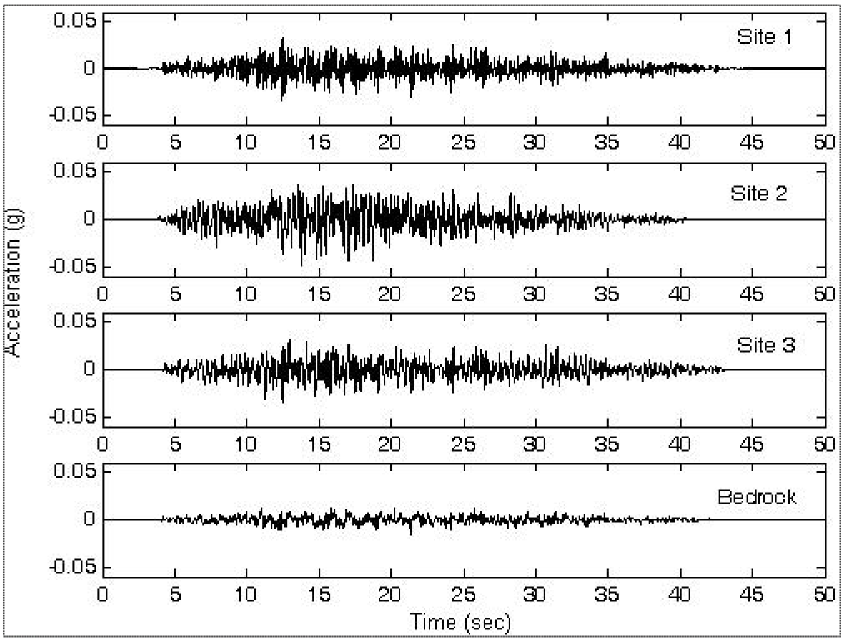

Fig. 4 Bedrock level and free-field motions at the top of three sites for a simulation of earthquake with M_w = 7.5

The variations of the average amplification ratios of 15 simulations for the three sites (with frequency) are obtained. As a typical case, the variations of average amplification ratios for the M_w = 8.5 earthquake are shown in Figure 5. Further, the average peak amplification ratios and the frequencies corresponding to the peak amplification ratios for the three sites are given in Table 5. It can be seen from the results that the peak amplification ratios as well as the frequencies at which the peak amplification ratios occur are quite different for the three sites.

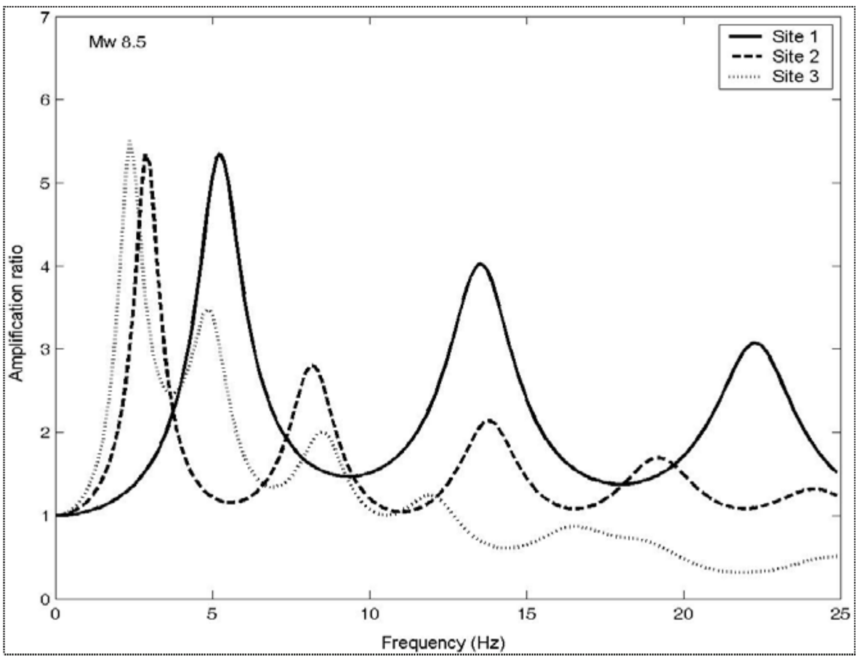

Fig. 5 Variations of average amplification ratios for the three sites for M_w = 8.5

Table 5: Average (over 15 Simulations) Fourier Amplification Ratios and Corresponding Frequencies for Site 1, Site 2 and Site 3

M_w	Fourier Amplification Ratio			Frequency of Amplification (Hz)		
	Site 1	Site 2	Site 3	Site 1	Site 2	Site 3
7.5	5.7	6.5	6.0	5.5	3.25	2.625
8.0	5.6	6.2	5.8	5.375	3.25	2.625
8.5	5.3	5.3	5.5	5.25	2.87	2.375

The average ratios of the peak ground accelerations (PGAs) of free-field motions to the PGAs of bedrock motions for the three sites are shown in Table 6. Also shown in Table 6 are the average PGAs for the 15 simulations of bedrock motions and free-field motions for Site 1, Site 2 and Site 3. It can be observed that the PGA amplifications at the three sites are different for the three earthquake magnitudes.

Table 6: Average PGAs of Bedrock Motions, and Average PGAs of Free-Field Motions and Average PGA Amplification Ratios for Site 1, Site 2 and Site 3

M_w	Average PGA (cm/s^2)				Average PGA Amplification Ratio		
	Bedrock Motion	Free-Field Motion					
		Site 1	Site 2	Site 3	Site 1	Site 2	Site 3
7.5	15.74	31.73	51.73	39.60	2.02	3.29	2.52
8.0	23.36	53.48	53.10	60.10	2.29	2.27	2.57
8.5	46.47	100.82	100.01	113.32	2.17	2.15	2.44

The 5%-damping response spectra for the 15 simulations of the free-field motions on the top of the three sites and the corresponding average spectra are obtained for all the three earthquake magnitudes. Typically for M_w = 8.0, these are shown for Site 2 in Figure 6. Further, the comparison of average response spectra for the three sites for the earthquake magnitudes M_w = 7.5, 8.0 and 8.5 are shown in Figures 7, 8 and 9, respectively. From these comparisons it can be inferred that the shapes of the response spectra vary quite significantly for the three sites under the same earthquake.

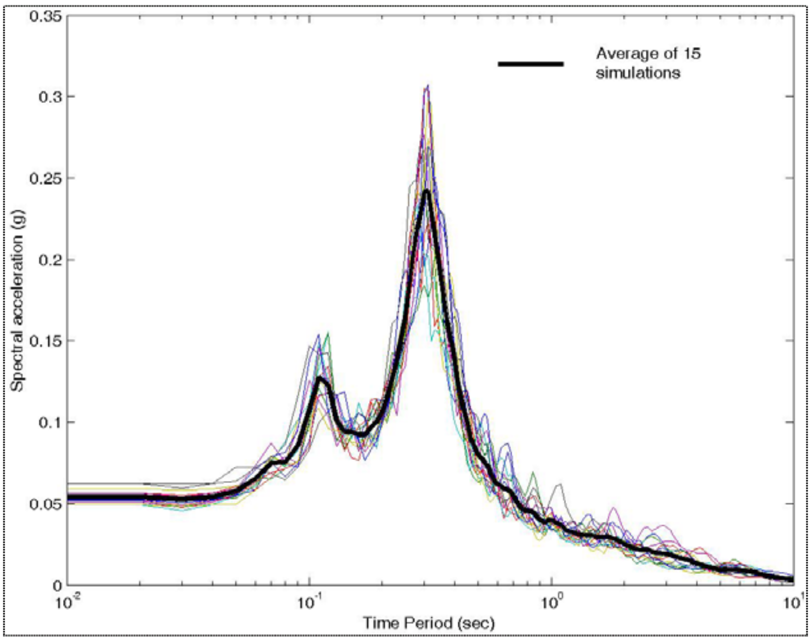

Fig. 6 5%-damping response spectra for the 15 simulations of free-field motions and average response spectrum for M_w = 8.0 and Site 2

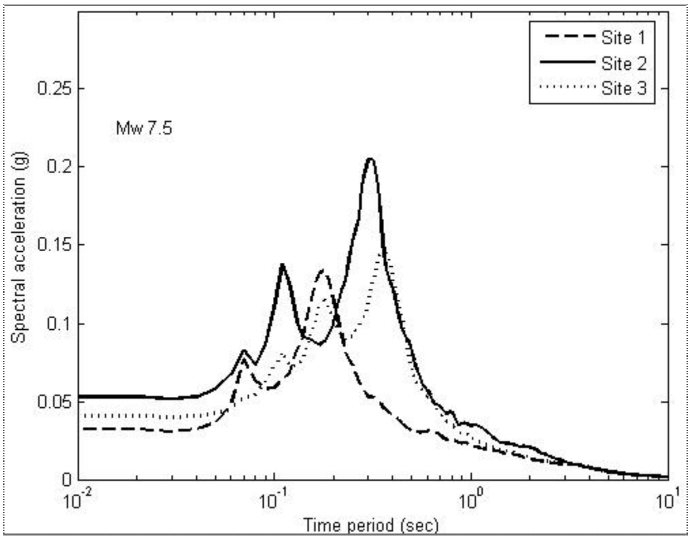

Fig. 7 Comparison of average response spectra for Site 1, Site 2 and Site 3 and M_w = 7.5

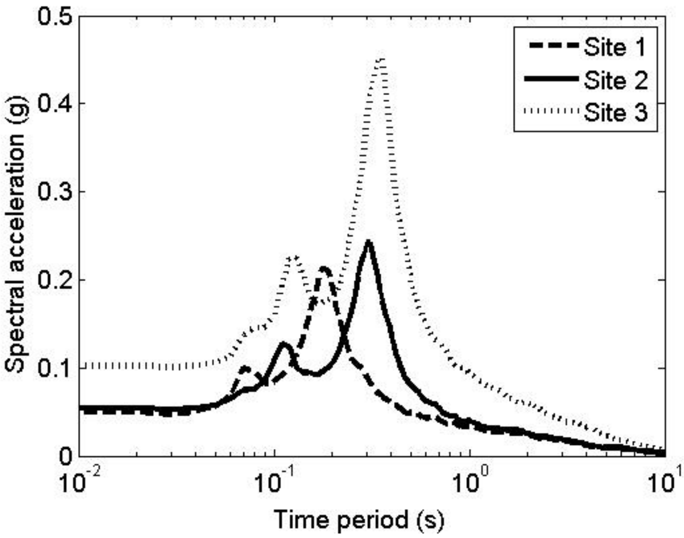

Fig. 8 Comparison of average response spectra for Site 1, Site 2 and Site 3 and M_w = 8.0

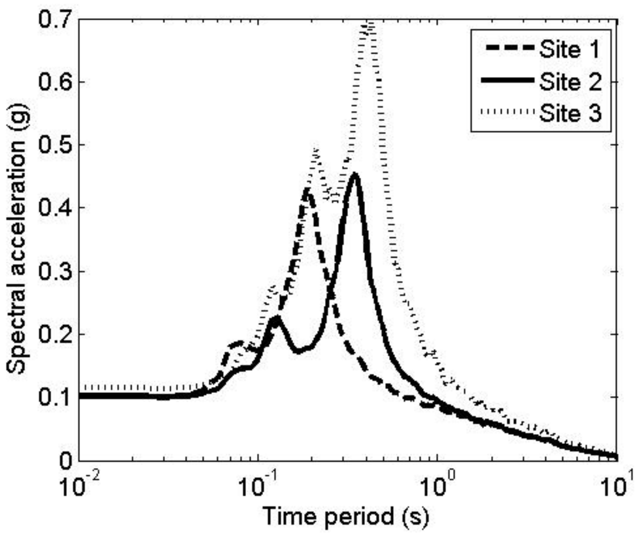

Fig. 9 Comparison of average response spectra for Site 1, Site 2 and Site 3 and M_w = 8.5

Major revisions have been taking place in seismic codes towards performance-based design (ATC, 1996; FEMA, 1997a; FEMA, 1997b). Response spectra form the basis for the demand curve in performance-based design and thus are of interest to structural engineers. The average response spectra of the three sites together with the average bedrock spectrum are represented in the Acceleration Displacement Response Spectrum (ADRS) format in Figures 10, 11 and 12, respectively. Typically it can be seen from Figures 10, 11 and 12 that for the same time period of the building (viz., T = 0.5 s) the spectral acceleration and spectral displacement are different for the three sites. This indicates that the same building will be subjected to different levels of damage during the same earthquake when situated on different sites in the Delhi region.

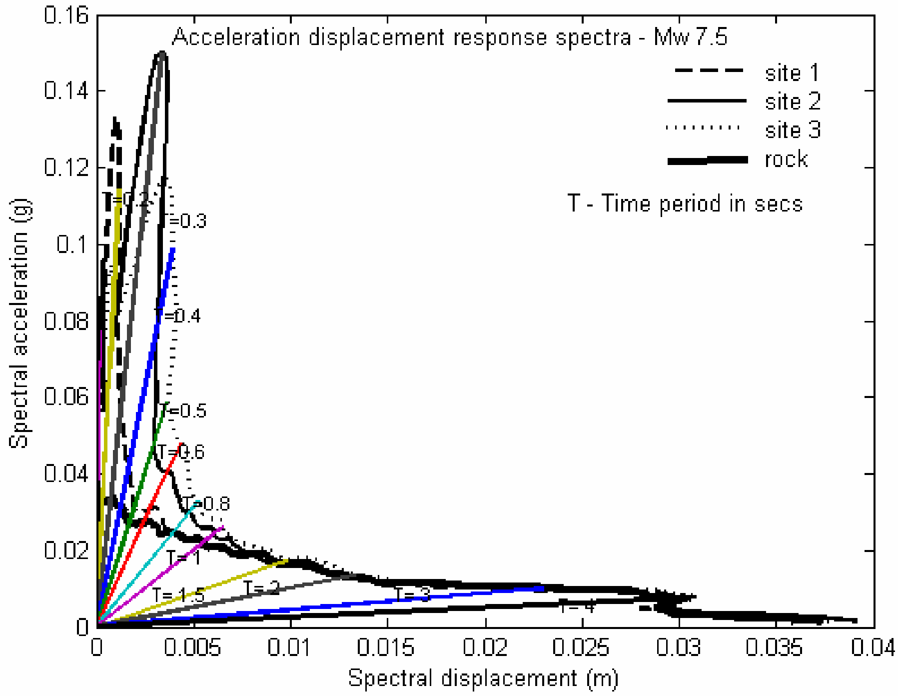

Fig. 10 Acceleration displacement response spectra for Site 1, Site 2 and Site 3 and M_w = 7.5

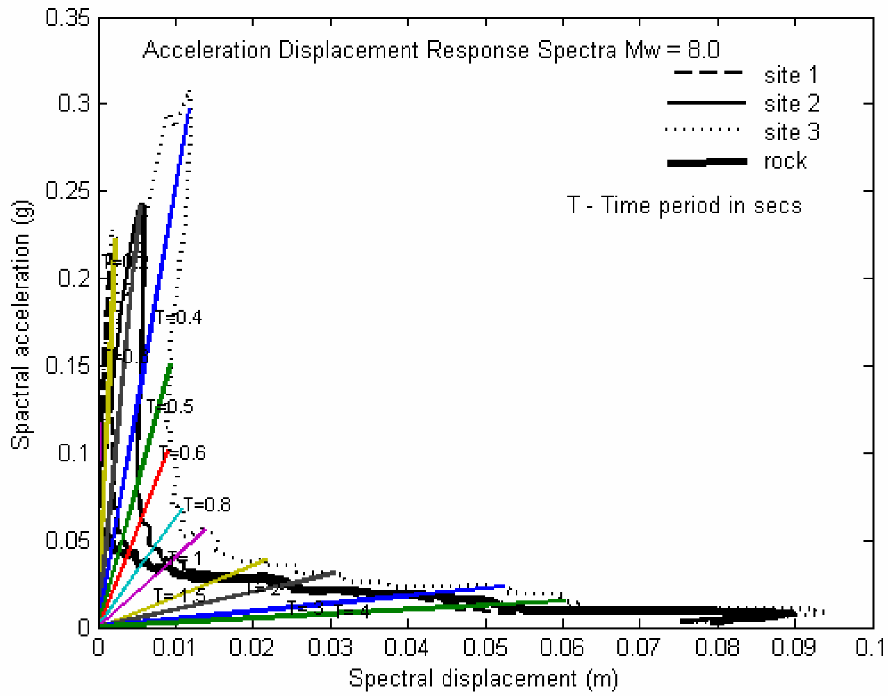

Fig. 11 Acceleration displacement response spectra for Site 1, Site 2 and Site 3 and M_w = 8.0

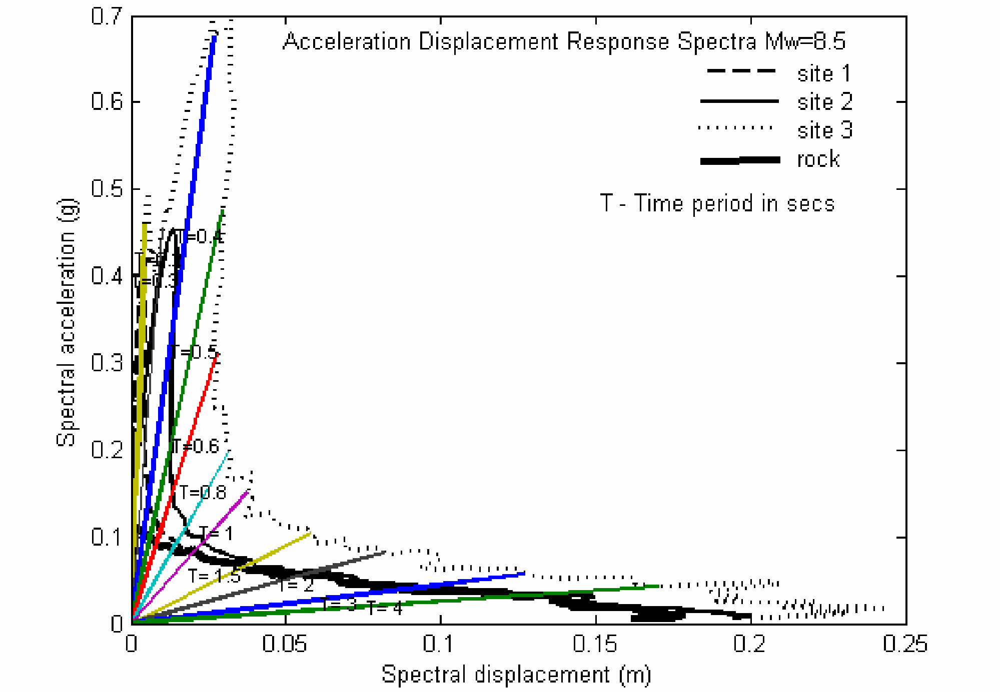

Fig. 12 Acceleration displacement response spectra for Site 1, Site 2 and Site 3 and M_w = 8.5

CONCLUSIONS

In this paper rock outcrop motions have been generated for Delhi for the scenario earthquakes of magnitudes M_w = 7.5, 8.0 and 8.5. Three actual soil sites (of medium soil) have been modeled and the free-field surface motions and the corresponding response spectra have been obtained. It has been observed that the PGA amplifications and the response spectra of the three sites are quite different from each other for the earthquakes considered. It is also clear from the response spectra in ADRS format that the performance of buildings will be different when situated on these soil sites. Based on the studies made, it can be concluded that it may be necessary to perform the site-specific analyses of buildings at the sites having medium types of soil as well.

ACKNOWLEDGEMENTS

The authors thank the anonymous reviewer and Dr. David M Boore for carefully reviewing the paper and improving the quality of the paper by providing critical comments and inputs.

REFERENCES

1. Aki, K. (1967). “Scaling Law of Seismic Spectrum”, Journal of Geophysical Research, Vol. 72, No. 4, pp. 1217–1231.
2. ATC (1996). “Seismic Evaluation and Retrofit of Concrete Buildings: Volume 1”, Report ATC-40, Applied Technology Council, Redwood City, U.S.A.
3. Atkinson, G.M. and Beresnev, I.A. (2002). “Ground Motions at Memphis and St. Louis from *M* 7.5-8.0 Earthquakes in the New Madrid Seismic Zone”, Bulletin of the Seismological Society of America, Vol. 92, No. 3, pp. 1015–1024.
4. Beresnev, I.A. and Atkinson, G.M. (1997). “Modeling Finite-Fault Radiation from the ω^n Spectrum”, Bulletin of the Seismological Society of America, Vol. 87, No. 1, pp. 67–84.
5. Beresnev, I.A. and Atkinson, G.M. (1998). “FINSIM—A FORTRAN Program for Simulating Stochastic Acceleration Time Histories from Finite Faults”, Seismological Research Letters, Vol. 69, No. 1, pp. 27–32.

6. Beresnev, I.A. and Atkinson, G.M. (2002). "Source Parameters of Earthquakes in Eastern and Western North America Based on Finite-Fault Modeling", Bulletin of the Seismological Society of America, Vol. 92, No. 2, pp. 695–710.
7. Bilham, R., Blume, F., Bendick, R. and Gaur, V.K. (1998). "Geodetic Constraints on the Translation and Deformation of India: Implication for Future Great Himalayan Earthquakes", Current Science, Vol. 74, No. 3, pp. 213–229.
8. BIS (2002). "IS 1893 (Part 1): 2002—Indian Standard Criteria for Earthquake Resistant Design of Structures, Part 1: General Provisions and Buildings (Fifth Revision)", Bureau of Indian Standards, New Delhi.
9. Boore, D.M. (1983). "Stochastic Simulation of High-Frequency Ground Motions Based on Seismological Models of the Radiated Spectra", Bulletin of the Seismological Society of America, Vol. 73, No. 6A, pp. 1865–1894.
10. Boore, D.M. (2003). "Simulation of Ground Motion Using the Stochastic Method", Pure and Applied Geophysics, Vol. 160, No. 3-4, pp. 635–676.
11. Boore, D.M. (2004). "Can Site Response be Predicted?", Journal of Earthquake Engineering, Vol. 8, No. S1, pp. 1–41.
12. Boore, D.M. and Atkinson, G.M. (1987). "Stochastic Prediction of Ground Motion and Spectral Response Parameters at Hard-Rock Sites in Eastern North America", Bulletin of the Seismological Society of America, Vol. 77, No. 2, pp. 440–467.
13. Boore, D.M. and Joyner, W.B. (1997). "Site Amplifications for Generic Rock Sites", Bulletin of the Seismological Society of America, Vol. 87, No. 2, pp. 327–341.
14. Borcherdt, R.D. (1994). "Estimates of Site-Dependent Response Spectra for Design (Methodology and Justification)", Earthquake Spectra, Vol. 10, No. 4, pp. 617–653.
15. Brune, J. (1970). "Tectonic Stress and the Spectra of Seismic Shear Waves from Earthquakes", Journal of Geophysical Research, Vol. 75, No. 26, pp. 4997–5009.
16. FEMA (1997a). "NEHRP Guidelines for the Seismic Rehabilitation of Buildings", Report FEMA-273, Federal Emergency Management Agency, Washington, DC, U.S.A.
17. FEMA (1997b). "NEHRP Commentary on the Guidelines for the Seismic Rehabilitation of Buildings", Report FEMA-274, Federal Emergency Management Agency, Washington, DC, U.S.A.
18. Govinda Raju, L., Ramana, G.V., Hanumantha Rao, C. and Sitharam, T.G. (2004). "Site-Specific Ground Response Analysis", Current Science, Vol. 87, No. 10, pp. 1354–1362.
19. Hanks, T.C. and Kanamori, H. (1979). "A Moment Magnitude Scale", Journal of Geophysical Research, Vol. 84, No. B5, pp. 2348–2350.
20. Hartzell, S.H. (1978). "Earthquake Aftershocks as Green's Functions", Geophysical Research Letters, Vol. 5, No. 1, pp. 1–4.
21. Herrmann, R.B. and Kijko, A. (1983). "Modeling Some Empirical Vertical Component L_g Relations", Bulletin of the Seismological Society of America, Vol. 73, No. 1, pp. 157–171.
22. Heuze, F., Archuleta, R., Bonilla, F., Day, S., Doroudian, M., Elgamal, A., Gonzales, S., Hoehler, M., Lai, T., Lavallee, D., Lawrence, B., Liu, P.-C., Martin, A., Matesic, L., Minster, B., Mellors, R., Oglesby, D., Park, S., Riemer, M., Steidl, J., Vernon, F., Vucetic, M., Wagoner, J. and Yang, Z. (2004). "Estimating Site-Specific Strong Earthquake Motions", Soil Dynamics and Earthquake Engineering, Vol. 24, No. 3, pp. 199–223.
23. ICC (2000). "International Building Code", International Code Council, Washington, DC, U.S.A.
24. Idriss, I.M. (1990). "Response of Soft Soil Sites during Earthquakes", Proceedings of the H.B. Seed Memorial Symposium, Berkeley, U.S.A., pp. 273–289.
25. Idriss, I.M. and Seed, H.B. (1970). "Seismic Response of Soil Deposits", Journal of the Soil Mechanics and Foundations Division, Proceedings of ASCE, Vol. 96, No. SM2, pp. 631–638.
26. Khattri, K.N. (1999). "An Evaluation of Earthquakes Hazard and Risk in Northern India", Himalayan Geology, Vol. 20, No. 1, pp. 1–46.

27. Lam, N.T.K., Wilson, J.L. and Chandler, A.M. (2001). "Seismic Displacement Response Spectrum Estimated from the Frame Analogy Soil Amplification Model", Engineering Structures, Vol. 23, No. 11, pp. 1437–1452.
28. Ordóñez, G.A. (2002). "SHAKE2000: A Computer Program for the I-D Analysis of Geotechnical Earthquake Engineering Problems—User's Manual", GeoMotions, LLC, Lacey, U.S.A.
29. Rao, H.Ch. and Ramana, G.V. (2004). "Correlation between Shear Wave Velocity and N value for Yamuna Sand of Delhi", Proceedings of the International Conference on Geotechnical Engineering, Sharjah, U.A.E., pp. 262–268.
30. Roumelioti, Z. and Beresnev, I.A. (2003). "Stochastic Finite-Fault Modeling of Ground Motions from the 1999 Chi-Chi, Taiwan, Earthquake: Application to Rock and Soil Sites with Implications for Nonlinear Site Response", Bulletin of the Seismological Society of America, Vol. 93, No. 4, pp. 1691–1702.
31. Schnabel, P.B., Lysmer, J. and Seed, H.B. (1972). "SHAKE: A Computer Program for Earthquake Response Analysis of Horizontally Layered Sites", Report UCB/EERC-72/12, University of California, Berkeley, U.S.A.
32. Seed, H.B. and Idriss, I.M. (1969). "Influence of Soil Conditions on Ground Motions during Earthquakes", Journal of the Soil Mechanics and Foundations Division, Proceedings of ASCE, Vol. 95, No. SM1, pp. 99–137.
33. Singh, S.K., Mohanty, W.K., Bansal, B.K. and Roonwal, G.S. (2002). "Ground Motion in Delhi from Future Large/Great Earthquakes in the Central Seismic Gap of the Himalayan Arc", Bulletin of the Seismological Society of America, Vol. 92, No. 2, pp. 555–569.
34. Tewari, H.C. and Kumar, P. (2003). "Deep Seismic Sounding Studies and Its Tectonic Implications", Journal of Virtual Explorer, Vol. 12, No. 1, pp. 30–54.
35. Vucetic, M. and Dobry, R. (1991). "Effect of Soil Plasticity on Cyclic Response", Journal of Geotechnical Engineering, ASCE, Vol. 117, No. 1, pp. 89–107.
36. Yoshida, N., Kobayashi, S., Suetomi, I. and Miura, K. (2002). "Equivalent Linear Method Considering Frequency Dependent Characteristics of Stiffness and Damping", Soil Dynamics and Earthquake Engineering, Vol. 22, No. 3, pp. 205–222.

ISET Journal of Earthquake Technology, Paper No. 511, Vol. 47, No. 2-4, June-Dec. 2010, pp. 75–85

INCLUSION OF $P-\Delta$ EFFECTS IN THE ESTIMATION OF HYSTERETIC ENERGY DEMAND BASED ON MODAL PUSHOVER ANALYSIS

Amarnath Roy Chowdhury and Siddhartha Ghosh

Department of Civil Engineering
Indian Institute of Technology Bombay
Mumbai-400076

ABSTRACT

The estimation of hysteretic energy demand is the first significant step in the energy-based seismic design of structures. The present paper extends a modal pushover analysis (MPA)-based energy demand estimation method to include the $P-\Delta$ effects in structures. The efficiency of the extended procedure is tested on three standard steel moment-resisting frames by comparing the estimates based on this method with the results from the nonlinear dynamic analyses of MDOF systems for several earthquakes. In addition, three non-standard frames with artificially increased susceptibility to $P-\Delta$ effects are also considered. Bias statistics are presented to show the effectiveness of the proposed method on including the $P-\Delta$ effects for both the standard and the non-standard designs. The $P-\Delta$ effects on the actual hysteretic energy demand of a structure are also studied. The MPA-based method including the $P-\Delta$ effects remains less demanding on computations and is also suitable for adopting in design guidelines.

KEYWORDS: Hysteretic Energy Demand, Modal Pushover Analysis, $P-\Delta$ Effect, Dynamic Stability, Energy-Based Seismic Design

INTRODUCTION

In recent years, many researchers have identified hysteretic energy demand or its equivalent parameters as the demand parameters that are most closely correlated to the seismic damage of structures (Zahrah and Hall, 1984; Fajfar, 1992; Manfredi, 2001). The hysteretic energy demand takes into account the effects of the duration of the earthquake ground motion and the cyclic-plastic deformation behavior of the structure. A monotonic demand parameter, such as peak inelastic drift or displacement, cannot represent this cumulative cyclic damage. A design approach based on hysteretic energy demand, thus, has the potential to account for the damage potential explicitly.

The necessity of an energy-based design procedure for future seismic design guidelines has been emphasized by many researchers, including a few attempts at providing a framework for such design procedures. The discussions of these efforts can be found in Ghosh and Collins (2006) and Prasanth et al. (2008). The estimation of hysteretic energy demand on structures is the first significant step in an energy-based design method. With the computing facilities available today, such estimation for a specific structure under certain earthquake ground motion is not difficult, even though this may be computation intensive. However, one has to apply the detailed method, i.e., the nonlinear response history analysis (NL-RHA) of a multi-degree-of-freedom (MDOF) model, for each individual structure separately. In addition, this method cannot use a single-degree-oscillator-based design/response spectrum, thus making the direct method unsuitable for incorporating in a general purpose design methodology based on hysteretic energy demand.

This paper investigates a simpler method for estimating hysteretic energy demand. It is an extension of the work by Prasanth et al. (2008) that used the concepts of modal pushover analysis (MPA) (Chopra and Goel, 2002; Goel and Chopra, 2004) for estimating hysteretic energy demand on MDOF systems. Prasanth et al. (2008) used multiple equivalent single-degree-of-freedom (ESDOF) systems for the modes of a structure. This MPA-based approximate method of estimating hysteretic energy demand was found to be very efficient for steel frame structures. However, this method did not consider the effects of gravity load and $P-\Delta$.

The $P-\Delta$ effects (i.e., the global/structure P-delta effects) are the second-order effects arising due to geometric nonlinearity in the static and dynamic analyses of structures under lateral loads, such as those due to earthquakes. These are secondary moment effects due to gravity loads combined with large inter-story deformations. These effects may significantly alter the response of an inelastic system susceptible to large deformations during the course of an earthquake. Gravity loads, acting through the large inter-story deformations, may even cause dynamic instability by reducing the lateral stiffness in a severe ground motion scenario (Bernal, 1998). The $P-\Delta$ effect can be very severe on flexible structures, such as steel moment-resisting frames, because those are subjected to large lateral displacements during a seismic shaking (Gupta and Krawinkler, 1999). A detailed review of research work on the various aspects of $P-\Delta$ effects on the seismic response of building structures is avoided in this article. Asimakopoulos et al. (2007) compiled a list of works available on $P-\Delta$ effects in structures. The present article proposes a modification on the method proposed by Prasanth et al. (2008) to account for the $P-\Delta$ effects and studies the effectiveness of the modified method for representative low-, mid- and high-rise steel frame building structures, by comparing MPA estimates with the results from the NL-RHA of a MDOF system. In addition, the effectiveness of the modified method is checked for non-standard designs that are specifically vulnerable to the $P-\Delta$ effects due to very high gravity loads. The primary focus of this paper is on measuring the effectiveness and on checking the robustness of the approximate method through various case studies. The $P-\Delta$ effects on the computed hysteretic energy demand are also studied. It may be noted that the objective here is not to find out how damage (in terms of hysteretic energy demand) is distributed in the structure. This paper follows the concept of using the overall energy demand in a structure as a design criterion, as proposed by previous researchers (Fajfar, 1992; Ghosh and Collins, 2006).

INCLUDING $P-\Delta$ EFFECTS IN AN MPA-BASED ANALYSIS

If large inelastic deformations occur during an earthquake, the $P-\Delta$ effects in a structure become significant as those further increase the displacements and may reduce the lateral load carrying capacity. Those may even result in the dynamic instability or the collapse of a story. Based on these considerations, the inclusion of $P-\Delta$ effects becomes necessary while estimating inelastic force and deformation parameters through nonlinear analysis (Gupta and Krawinkler, 1999).

In MPA (Chopra and Goel, 2002) the elastic mode shapes and frequencies are used to formulate a nonlinear ESDOF model for each mode. The nonlinear characteristics of each mode, such as yield point and strain hardening stiffness ratio, are obtained through a nonlinear static pushover analysis using a mode-specific lateral force distribution. The use of multiple modal ESDOF systems in MPA overcomes the limitation of traditional pushover analysis of not being able to account for the higher-mode effects. MPA was used for estimating seismic force and displacement demands on nonlinear (inelastic) as well as linear elastic MDOF systems with sufficient closeness to the results obtained from a response history analysis. The advantage of MPA is that it achieves this degree of accuracy without losing the conceptual simplicity and computational attractiveness of the traditional pushover procedure. Goel and Chopra (2004) modified this by including $P-\Delta$ effects in the nonlinear static pushover analyses. The modified method was tested on the 9- and 20-story SAC steel frames from Boston, Los Angeles and Seattle in USA. It was observed that $P-\Delta$ effects increased bias in the MPA-based estimation of story drift ratios (to over 40% for the 20-story building at Los Angeles), where bias was defined as the ratio of the NL-RHA-based estimation of a parameter to the MPA-based estimation of that parameter.

A similar modification (Goel and Chopra, 2004) is attempted here for the MPA-based estimation of hysteretic energy demand. The $P-\Delta$ effects are included in the nonlinear pushover analysis corresponding to each mode. The lateral force distribution $\{f_n\}$ for the *n*th-mode pushover analysis is obtained based on the *n*th mode shape, after normalizing $[m]\{\phi_n\}$ to a unit base shear (i.e., $\{f_n\}$ = $[m]\{\phi_n\}/\{\iota\}^T[m]\{\phi_n\}$), where $[m]$ is the mass matrix, $\{\phi_n\}$ is the *n*th mode shape normalized to a unit roof displacement component, and $\{\iota\}$ is the influence vector. For each mode, the pushover analysis is carried out to achieve a maximum interstory drift of 2.5%. As mentioned in similar works earlier (Ghosh and Collins, 2006; Prasanth et al., 2008), the results do not change significantly if a higher value of maximum drift is considered in the pushover analyses including $P-\Delta$ effects. The base shear (i.e., V_n) versus roof displacement (i.e., D_n) "pushover" curve is approximated by a bilinear function by equating the areas underneath the two curves. This bilinear curve gives the elastic stiffness K_{pon}, the yield displacement D_{yn} (= V_{yn}/K_{pon}) and the strain hardening stiffness ratio α_{kn}, from which critical parameters for the *n*th-mode equivalent system are obtained as described by Prasanth et al. (2008). The inclusion of $P-\Delta$ effects in the pushover analysis changes the parameters for the corresponding modal ESDOF system. It primarily changes the strain-hardening stiffness ratio α_{kn} and yield force V_{yn}, though it may also affect the elastic parameters, such as stiffness K_n and period T_n (or frequency ω_n). The governing equation of motion for the *n*th modal ESDOF system subjected to the ground acceleration $\ddot{u}_g$ is written as

$$\ddot{q}_n + 2\xi_n\omega_n\dot{q}_n + \omega_n^2 G_n\left(q_n, \operatorname{sgn}\dot{q}_n\right) = -\Gamma_n\ddot{u}_g \tag{1}$$

where ξ_n is the modal damping ratio, G_n expresses the force-deformation relation based on the bilinearized pushover plot, and Γ_n is the participation factor for the *n*th mode given by

$$\Gamma_n = \frac{\{\phi_n\}^{\mathrm{T}}[m]\{\iota\}}{\{\phi_n\}^{\mathrm{T}}[m]\{\phi_n\}} \tag{2}$$

The hysteretic energy demand E_{nh} in each mode is obtained by solving the nonlinear dynamic relation of Equation (1). Since E_{nh} is a cumulative (and non-decreasing) function in time, the peak hysteretic energy will always occur at the end of the analysis. A simple way to combine the individual E_{nh} values is to add those together. However, this is an approximation because this ignores any coupling that may occur in the inelastic domain (Prasanth et al., 2008).

The geometric nonlinearity due to flexural deformations within a member, or $P-\delta$ effects (i.e., the member P-delta effects), are not considered here because the focus is on the overall building response. Adam and Krawinkler (2004) found this phenomenon to be mostly insignificant for the overall seismic response of building structures.

CASE STUDY 1: SAC STEEL FRAMES IN LOS ANGELES

In order to test the effectiveness of the modified MPA-based hysteretic energy demand estimation method, it is used to predict energy demands for the 3-, 9- and 20-story "pre-Northridge" SAC steel moment frame buildings in Los Angeles, USA (Gupta and Krawinkler, 1999), subjected to 21 ground motion records. These buildings are selected for this case study because they represent standard earthquake-resistant designs and have been used in numerous research studies. Based on linear elastic static considerations, these buildings are not expected to show significant susceptibility to $P-\Delta$ effects. A story-specific stability coefficient is used, similar to Equation (4.1) in the report by Gupta and Krawinkler (1999), to measure this susceptibility based on a linear static pushover analysis with the IBC 2006-based lateral force distribution (ICC, 2006):

$$\theta_i = \frac{P_i\Delta_i}{V_i h_i} \tag{3}$$

Here, P_i is the total vertical load above the floor level i, Δ_i is the relative deformation at the *i*th story, V_i is the *i*th story shear, and h_i is the *i*th story height. The maximum stability coefficients obtained for the example 3-, 9- and 20-story buildings are 0.030, 0.069 and 0.112, respectively. A value of 0.1 is often cited as a limit above which $P-\Delta$ effects should be considered in design. The effectiveness of the method proposed by Prasanth et al. (2008) is also tested for another set of buildings where significant $P-\Delta$ effects are expected. This will be discussed in the next section.

It may be mentioned that the use of a stability coefficient similar to Equation (3) to predict the vulnerability of a structure to $P-\Delta$ effects is highly questionable. FEMA-355C (FEMA, 2000) states that it "provides inadequate information on the occurrence of a negative post-mechanism stiffness and against excessive drifting of the seismic response." This coefficient cannot properly account for the inelastic and dynamic effects. Gupta and Krawinkler (1999) pointed out that $P-\Delta$ effects are very sensitive to ground motion characteristics, once negative post-yield stiffness is attained. Despite these shortcomings, it is used in this paper because of its familiarity to engineers and researchers.

The details of Los Angeles SAC buildings, including gravity loads, can be obtained from the previous publications (Gupta and Krawinkler, 1999; Ghosh, 2003) and are, therefore, avoided here. The details of the ground motion records considered, which include the 18 records used by Prasanth et al. (2008) and three additional records (from 1971 San Fernando earthquake, 1978 Tabas earthquake and 1989 Loma Prieta earthquake), are available in a detailed report (Roy Chowdhury, 2008). Only the North-South moment frames of the (symmetric) Los Angeles buildings are considered for static pushover and nonlinear response history analyses. These analyses are performed using the software DRAIN-2DX (Prakash et al., 1993). The analysis methods and considerations are the same as those adopted by Prasanth et al. (2008), except for including $P-\Delta$ effects in the pushover analyses as discussed in the previous section. The nonlinear response-history analyses are carried out by applying the earthquake accelerations at the base of the 2-D frames. The frame members are modeled by using the plastic hinge beam-column element (of Type 02), with rigid-plastic hinges at their ends. The P-M interaction is considered for the hinge capacity. The material behaviour is assumed to be bilinear with 5% strain-hardening stiffness ratio. The strength and stiffness degradations are neglected in the hysteretic behaviour. The flexibility of the joint panel zones and the lateral stiffness of the gravity frames are not considered. A Rayleigh damping of 5% is assumed (for the first two modes) for the NL-RHA. Although Prasanth et al. (2008) recommended the use of only the first three modes, even for the 9- and 20-story buildings, here the first five modes are considered for energy estimations while including $P-\Delta$ effects. Various results from this set of case studies are discussed next.

The $P-\Delta$ effects are found to be significant on some ESDOF parameters, but primarily on the strain-hardening stiffness ratio α_{kn}. Those also affect the other parameters, such as the yield force V_{yn} and stiffness K_n. Table 1 presents, for example, the changes in some of these parameters due to the inclusion of $P-\Delta$ effects in pushover analyses for the first five modes of the 20-story frame. The $P-\Delta$ effects are most significant for the first mode. These observations are similar to those reported by Goel and Chopra (2004).

Table 1: ESDOF Parameters for First Five Modes of 20-Story SAC Steel Frame

Mode	Without $P-\Delta$ Effects			With $P-\Delta$ Effects		
	α_{kn} (%)	V_{yn} (kN)	T_n (s)	α_{kn} (%)	V_{yn} (kN)	T_n (s)
1	13.4	2821	3.81	–9.20	2439	3.99
2	3.00	8200	1.32	3.74	6562	1.32
3	4.76	10220	0.766	3.24	9889	0.771
4	5.85	14370	0.543	4.87	14010	0.552
5	9.10	19490	0.414	8.18	19030	0.414

Table 2: Bias Statistics in Estimation of Hysteretic Energy Demand for Original SAC Steel Frames

	3-Story		9-Story		20-Story	
	Without $P-\Delta$	With $P-\Delta$	Without $P-\Delta$	With $P-\Delta$	Without $P-\Delta$	With $P-\Delta$
Mean	1.08	1.13	1.11	1.12	1.38	1.05
SD	0.057	0.066	0.150	0.147	0.412	0.228
CoV	0.053	0.059	0.135	0.131	0.299	0.218
Maximum	1.18	1.25	1.44	1.44	2.56	1.81
Minimum	0.954	1.00	0.939	0.958	0.906	0.767

The accuracy of the MPA-based estimation is measured by using the statistics of a bias factor defined as

$$N_{\text{MPA}} = \frac{E_{\text{NL-RHA}}}{E_{\text{MPA}}} \tag{4}$$

where $E_{\text{NL-RHA}}$ is the hysteretic energy demand based on the nonlinear response history analysis of the MDOF model of the actual structure, and E_{MPA} is the hysteretic energy demand based on the MPA-based method. This bias factor is calculated for each earthquake, and its statistics (i.e., mean, standard deviation, coefficient of variation, and maximum and minimum values) are provided in Table 2. Table 2 also presents the results for the same buildings when no $P-\Delta$ effects are considered (neither in NL-RHA nor in MPA). In addition, Figure 1 provides simple scatter plots that compare the values of $E_{\text{NL-RHA}}$ and E_{MPA} for each earthquake, when $P-\Delta$ effects are included. The diagonal line across a scatter plot represents the perfect agreement between the NL-RHA and the approximate analysis technique. These scatter plots provide an easy estimation of how effective the MPA method is when $P-\Delta$ effects are considered.

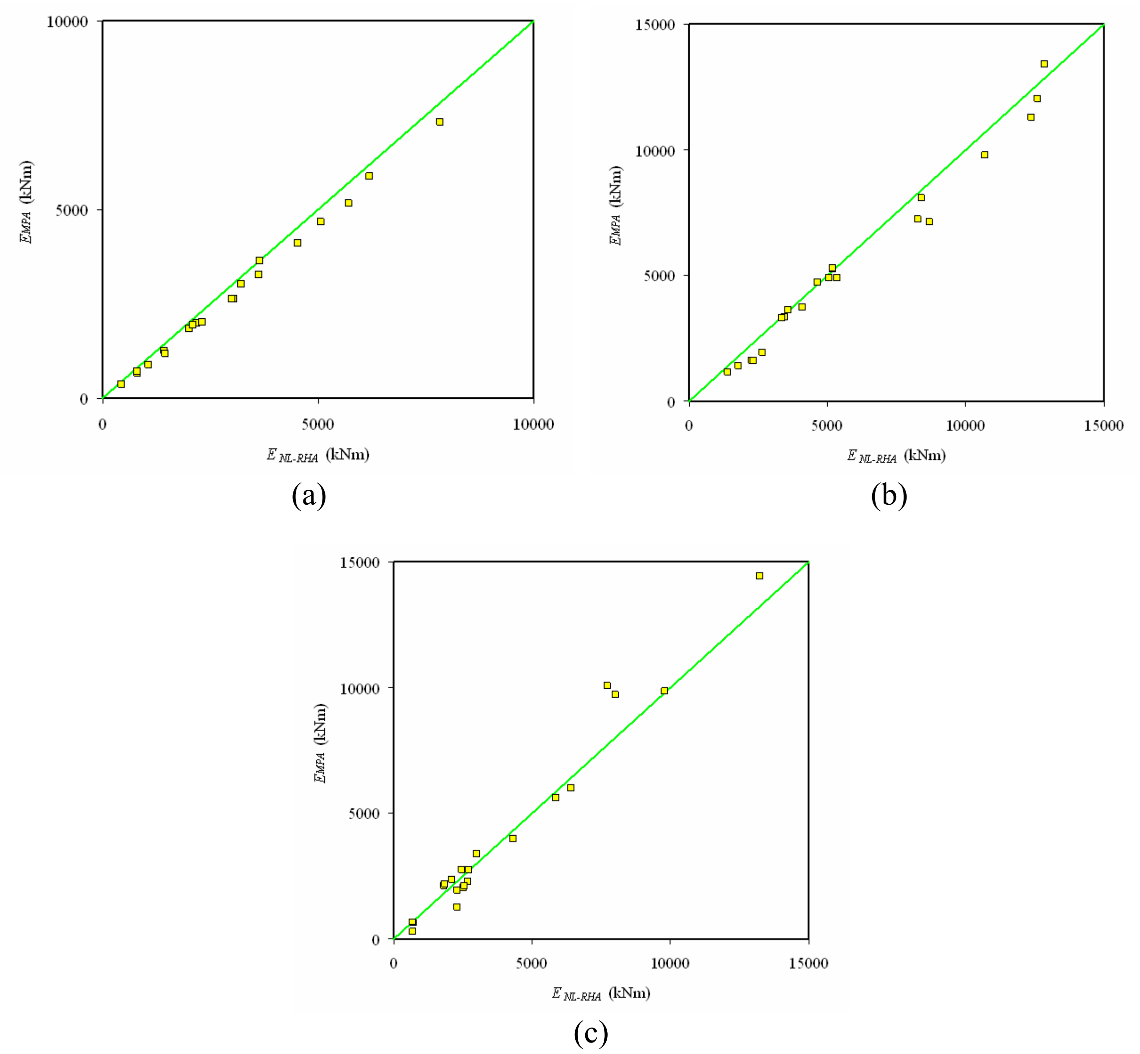

Fig. 1 Scatter plots comparing E_{MPA} with $E_{\text{NL-RHA}}$, with $P-\Delta$ effects included, for the original SAC steel (a) 3-story, (b) 9-story and (c) 20-story buildings

The scatter plots and Table 2 show very clearly that the MPA-based method of hysteretic energy demand, on including the $P-\Delta$ effects, provides estimates that are comparable to the results from the "exact" NL-RHA for most of the cases considered. The mean bias is close to its ideal value of 1.0 and the scatter is also low for all the three frames. The largest discrepancies occur for the 20-story building, as also observed by Goel and Chopra (2004) for the MPA-based displacement estimation.

Table 3 provides a summary of the modal contributions of each ESDOF system to the E_{MPA} estimates presented in Figure 1(c) for the 20-story building. These results show that considering only the first three modes is sufficient even for the 20-story building. For many records, only the first mode contributes significantly. However, for a small number of records, the 2nd- and 3rd-mode contributions are also significant. In fact, the 2nd-mode contribution is more than the 1st-mode contribution in some cases. Prasanth et al. (2008) also observed similar results for these specific records while estimating the hysteretic energy demand for these frames without the $P-\Delta$ effects. As discussed in their paper, these interesting results are attributed to the unique characteristics and frequency content of the input ground motion records.

The level of accuracy, as measured in terms of the mean bias presented in Table 2, reduces on including the $P-\Delta$ effects by 4.8% and 0.89% for the 3- and 9-story frames, respectively. This may be due to the fact that $P-\Delta$ effects, based on their stability coefficients, are expected to be insignificant for these buildings. For the 20-story frame, on the other hand, the level of accuracy improves by 24%. It is difficult to ascertain any specific reason for this improvement. Prasanth et al. (2008) observed that when no $P-\Delta$ effects are considered, the MPA-based method underestimates the energy demand (on average), and the error (or the degree of underestimation) increases for higher buildings. It was suspected that the inability of the MPA-based method to account for the inelastic coupling of modes, which become more significant for the 20-story frame, is the reason for this underestimation. As shown later in Figure 4(a), the actual hysteretic energy demand $E_{\mathrm{NL\text{-}RHA}}$ on these frames does not change significantly on the inclusion or exclusion of the $P-\Delta$ effects. On considering the improvements in the MPA-based estimation, while including $P-\Delta$ effects for the 20-story frame, it can be conjectured that the effect of accounting for the $P-\Delta$ phenomenon in the MPA-based method is additive in terms of hysteretic energy demand on this structure (i.e., the hysteretic energy demand increases if $P-\Delta$ effects are included in the MPA-based method).

Table 3: Mode-wise Distribution of Hysteretic Energy Demand for SAC Steel 20-Story Building

Ground Motion Record	E_{nh}/E_{MPA} (with $E_{\mathrm{MPA}} = \sum_{n=1}^{5} E_{nh}$)				
	Mode 1 (%)	Mode 2 (%)	Mode 3 (%)	Mode 4 (%)	Mode 5 (%)
s640r005	100	0	0	0	0
s503r005	100	0	0	0	0
s065r005	97.9	2.06	0	0	0
s621r004	100	0	0	0	0
s050r005	89.9	10.1	0	0	0
s212r008	100	0	0	0	0
s305r008	72.1	27.9	0	0	0
s549r009	94.3	5.70	0	0	0
nr	41.4	53.2	5.38	0	0
ns	30.4	67.1	2.49	0	0
chy08036	16.2	81.5	2.27	0	0
chy0809	0	74.4	25.6	0	0
tcu0659	92.7	7.27	0	0	0
syl90	100	0	0	0	0
newh360	62.9	37.1	0	0	0
nh	67.1	32.9	0	0	0
syl360	67.6	32.4	0	0	0
tcu06536	90.9	9.07	0	0	0

lgp00	82.5	14.0	3.45	0	0
pcd164	54.3	45.7	0	0	0
tabln	84.6	15.4	0	0	0

The mean ratio of E_{MPA} with and without $P-\Delta$ effects is found to be 0.979, 0.867 and 1.16, respectively, for the 3-, 9-, and 20-story frames. The primary reason for this increase in E_{MPA} for the 20-story frame is the level of reduction in the ESDOF parameter α_{kn}. For example, for the 1st-mode ESDOF system, α_{kn} changes from 13.4% to –9.20% for the 20-story frame, from 11.8% to 2.88% for the 9-story frame, and from 11.4% to 8.91% for the 3-story frame. A simple study is performed to monitor the effect of change in α_{kn} on the hysteretic energy demand on an inelastic SDOF system. For this, two SDOF systems (one having the properties corresponding to the 1st modal ESDOF system of the 20-story frame, and the other corresponding to the 1st modal ESDOF system of the 9-story frame) subjected to the selected set of 21 earthquake records are analyzed and the hysteretic energy demand E_h is monitored with varying α_{kn} values. Figure 2 illustrates the variation in E_h (as normalized by E_h at α_{kn} = 0) with α_{kn} (the thick unbroken lines represent the mean values for all the records). This illustration shows that the variation in E_h changes with the earthquake record and with the SDOF system considered. As mentioned earlier, the $P-\Delta$ effects become very sensitive to ground motion characteristics, once the negative post-yield stiffness is attained. The mean curves show that, on average, E_h increases when there is a decrease in α_{kn} in the range of negative post-yield stiffness. For the 1st modal ESDOF of the 20-story frame, this increase occurs for a decrease in α_{kn} from 10% to –20%. With the change in the other ESDOF parameters being almost insignificant, a definite increase in hysteretic energy demand occurs when the reduction in the post-yield stiffness is more and to the range of 0% and below, i.e., for the high-rise frames having high stability coefficients.

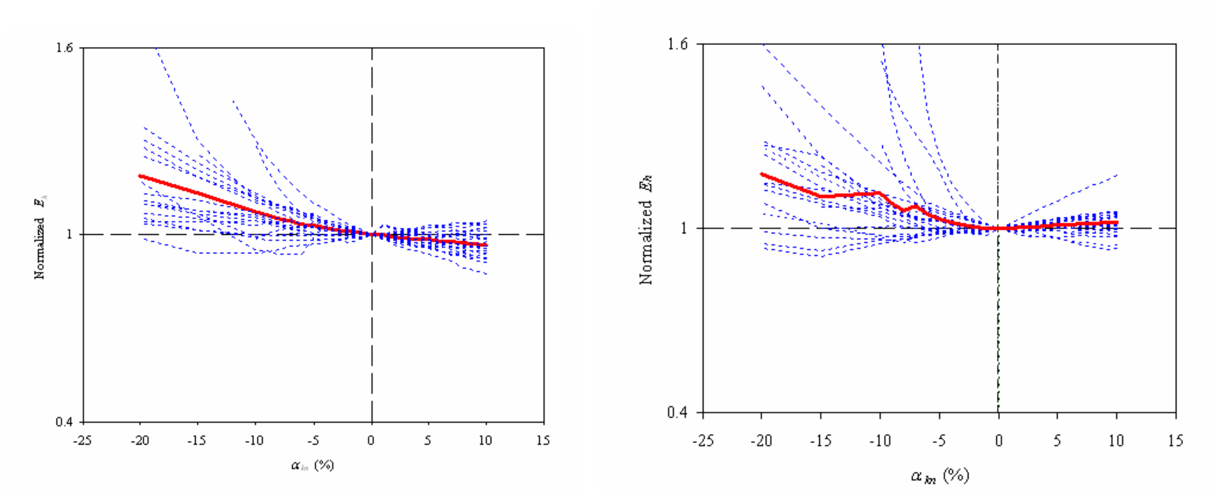

(a) (b)

Fig. 2 Variation of hysteretic energy demand (as normalized by E_h at $\alpha_{kn}=0$) with α_{kn} under 21 records (and the mean variation) for the 1st modal ESDOF systems of the (a) 20-story and (b) 9-story frames (the dashed lines represent results for the individual earthquakes and the solid line represents their mean)

CASE STUDY 2: BUILDINGS WITH INCREASED $P-\Delta$ EFFECTS

The MPA-based method proposed by Prasanth et al. (2008) for estimating hysteretic energy demand is also tested for the building frames susceptible to increased $P-\Delta$ effects during large earthquakes. For this case study of non-standard designs, the 3-, 9- and 20-story “pre-Northridge” SAC steel frames in Los

Angeles are again considered, but with artificially increased gravity loads (along with a suitable increase in inertial masses for the response-history analyses). The modified 3-, 9- and 20-story frames have maximum stability coefficients of 0.060, 0.137 and 0.168, respectively, as per Equation (3). It may be noted that the modified 3-story frame with the increased mass has a stability coefficient less than what is conventionally accepted as the minimum value (= 0.1) for having significant $P-\Delta$ effects. The 9- and 20-story frames with artificially increased stability coefficients become unstable (and the DRAIN-2DX solver fails to converge) for several large-magnitude earthquakes considered in the previous section. Also, the MPA-based method fails to deliver any results for some earthquakes as a very high negative strain-hardening stiffness of the modal ESDOF system causes the collapse of the frames. For example, the 1st-mode ESDOF system for the modified 20-story frame has α_{kn} = −30%, leading to a zero force carrying capacity under several earthquake records. These unstable cases are excluded from the results to follow. Similar cases of instability were also reported by previous researchers (Goel and Chopra, 2004) for the MPA-based displacement estimation.

The bias statistics summary for the above estimates, based on all 21 records for the 3-story frame, 14 records for the 9-story frame, and 9 records for the 20-story frame, is presented in Table 4. These results (see Table 4 and the scatter plots in Figure 3) show that the MPA-based method of estimating hysteretic energy works quite well even for those systems where $P-\Delta$ effects are exaggerated. The mean bias for the modified 9-story frame is at the same level as that for the original 9-story frame discussed in the previous section. For the modified 3-story frame, the estimates are good, with the level of accuracy slightly deteriorating from that of the original SAC frame. However, for the modified 20-story frame (with a very high stability coefficient), the mean bias goes down to 0.789. This may be due to the additive effect of significant $P-\Delta$ phenomenon on the SDOF energy demand for the MPA-based method, as discussed in the previous section (α_{kn} was observed to be −30% for the 1st modal ESDOF system of the modified 20-story frame). Overall, the results (with mean bias close to 1.0 and low coefficients of variation) show that the MPA-based method is effective even for the non-standard designs with very high stability coefficients. The discrepancies introduced by the inclusion of the $P-\Delta$ effects in the MPA-based hysteretic energy demand are lower than those for the MPA-based displacement estimation (Goel and Chopra, 2004). It may be mentioned here that the number of samples considered for these results, specifically for the modified 20-story frame, is small and that conclusions drawn here may need modifications based on a larger sample size.

Table 4: Bias Statistics in Estimation of Hysteretic Energy Demand for Modified 3-, 9- and 20-Story Frames

	3-Story[a]		9-Story[b]		20-Story[c]	
	Without $P-\Delta$	With $P-\Delta$	Without $P-\Delta$	With $P-\Delta$	Without $P-\Delta$	With $P-\Delta$
Mean	1.21	1.20	1.18	1.13	1.13	0.789
SD	0.164	0.223	0.159	0.141	0.275	0.085
CoV	0.136	0.186	0.135	0.125	0.244	0.107
Maximum	1.76	1.78	1.47	1.38	1.81	0.895
Minimum	1.05	0.67	1.02	0.935	0.903	0.674

[a] Based on 21 records
[b] Based on 14 records (7 records excluded due to instability)
[c] Based on 9 records (12 records excluded due to instability)

$P-\Delta$ EFFECTS ON HYSTERETIC ENERGY DEMAND

The effects of including the $P-\Delta$ behaviour on the actual hysteretic energy demand on a structure, as obtained from the NL-RHA of the MDOF model, are also studied for the three original SAC steel frames and the corresponding modified frames for the same set of acceleration records. Gupta and

Krawinkler (1999), based on their study of SAC steel frames, concluded that the dynamic effects of $P-\Delta$ behaviour can be additive or subtractive in terms of inelastic displacement demand (unlike the static effects which are always additive). However, there is no specific data available in the published literature on quantifying $P-\Delta$ effects in terms of hysteretic energy demand. Based on the results for the three original SAC steel frames, the $P-\Delta$ effects have almost no impact (as the mean ratio of $E_{\text{NL-RHA}}$ with $P-\Delta$ effects to that without $P-\Delta$ effects is 0.97 for the three frames together, with a standard deviation of 0.057) on the hysteretic energy demand for the whole frame. The scatter plot in Figure 4(a) illustrates this fact for all the three frames. For the modified 3-, 9- and 20-story frames with higher stability coefficients, the $P-\Delta$ effects are slightly more significant; however, there is no specific trend of increase or decrease in the energy demand, with the average demand remaining almost the same (see Figure 4(b); the mean ratio of $E_{\text{NL-RHA}}$ with $P-\Delta$ effects to that without $P-\Delta$ effects is 0.962 for the three frames together, with a standard deviation of 0.117).

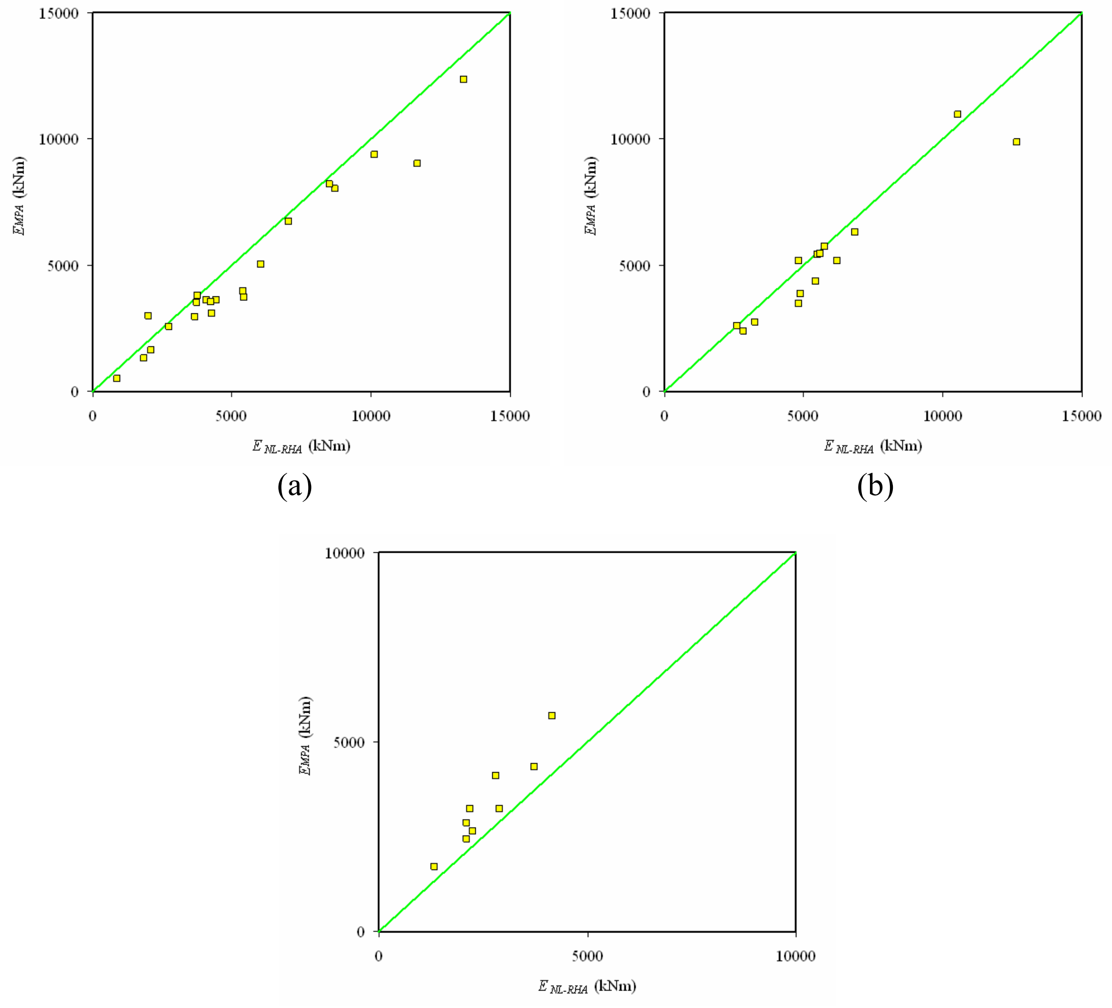

Fig. 3 Scatter plots comparing E_{MPA} with $E_{\text{NL-RHA}}$ for the (a) 3-story, (b) 9-story and (c) 20-story buildings with increased stability coefficient

SUMMARY AND CONCLUSIONS

A MPA-based hysteretic energy demand estimation technique has been extended in this paper to include the $P-\Delta$ effects in structures. The modified method has been tested on three low-to-high-rise steel frames conforming to design standards and on three non-standard low-to-high-rise steel frames with relatively high susceptibility to $P-\Delta$ effects. The $P-\Delta$ effects on the hysteretic energy demand (as obtained from the NL-RHA of the MDOF system) have also been studied.

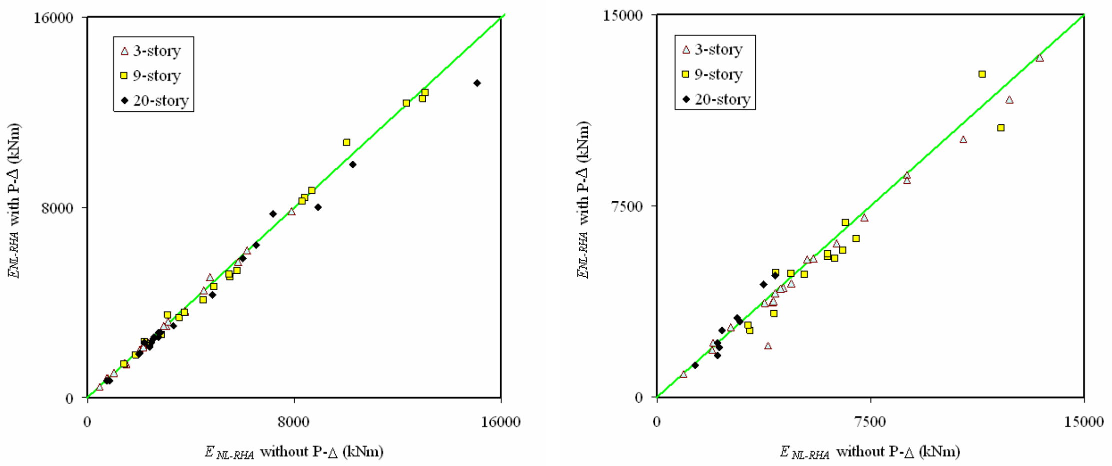

(a) (b)

Fig. 4 Comparison of $E_{\text{NL-RHA}}$ with and without $P-\Delta$ effects for the (a) original SAC steel frames, and the (b) modified frames with increased stability coefficients

The following general conclusions have been drawn based on the study presented in this article:

- The procedure proposed by Prasanth et al. (2008) remains a simple and effective method of estimating hysteretic energy demand on a structure even when the $P-\Delta$ effects are included.
- Based on the analyses of the 3-, 9- and 20-story SAC steel buildings, this procedure has been found to provide consistently good estimates of hysteretic energy demand, with the level of accuracy slightly increasing for taller frames.
- The MPA-based method also works well for non-standard designs where very high $P-\Delta$ effects are expected. The level of accuracy however goes down when the stability coefficient is increased to a very high value.
- The $P-\Delta$ effects may increase or decrease the value of energy demand estimated by using MPA (i.e., E_{MPA}), depending on the amount of negative post-yield stiffness caused by those effects.
- Based on NL-RHA, the $P-\Delta$ effects do not appear to significantly affect the hysteretic energy demand of a frame. The $P-\Delta$ effects on hysteretic energy demand increase for the buildings with large stability coefficients; however, there is no specific trend of increase or decrease in the demand.

These conclusions are based on the two sets of case studies conducted herein. The future extensions of this work may primarily focus on (a) estimating member/story-level hysteretic energy demands, and on (b) estimating energy demands for other structures with different hysteretic behavior (such as reinforced concrete buildings).

ACKNOWLEDGEMENTS

The authors would like to acknowledge Dr. Kevin R. Collins, Associate Professor, Valley Forge Military Academy and College, USA for his valuable suggestions on modifying the scope of this work. The authors also thank the reviewers of the paper for their time and valuable comments that have helped in enhancing its contents.

REFERENCES

1. Adam, C. and Krawinkler, H. (2004). "Large Displacement Effects on Seismically Excited Elastic-Plastic Frame Structures", Asian Journal of Civil Engineering (Building and Housing), Vol. 5, No. 1-2, pp. 41–55.

2. Asimakopoulos, A.V., Karabalis, D.L. and Beskos, D.E. (2007). "Inclusion of $P-\Delta$ Effect in Displacement-Based Seismic Design of Steel Moment Resisting Frames", Earthquake Engineering & Structural Dynamics, Vol. 36, No. 14, pp. 2171–2188.
3. Bernal, D. (1998). "Instability of Buildings during Seismic Response", Engineering Structures, Vol. 20, No. 4-6, pp. 496–502.
4. Chopra, A.K. and Goel, R.K. (2002). "A Modal Pushover Analysis Procedure for Estimating Seismic Demands for Buildings", Earthquake Engineering & Structural Dynamics, Vol. 31, No. 3, pp. 561–582.
5. Fajfar, P. (1992). "Equivalent Ductility Factors, Taking into Account Low-Cycle Fatigue", Earthquake Engineering & Structural Dynamics, Vol. 21, No. 10, pp. 837–848.
6. FEMA (2000). "State of the Art Report on Systems Performance of Steel Moment Frames Subject to Earthquake Ground Shaking", Report FEMA-355C, Federal Emergency Management Agency, Washington, DC, U.S.A.
7. Ghosh, S. (2003). "Two Alternatives for Implementing Performance-Based Seismic Design of Buildings—Life Cycle Cost and Seismic Energy Demand", Ph.D. Thesis, Department of Civil and Environmental Engineering, University of Michigan, Ann Arbor, U.S.A.
8. Ghosh, S. and Collins, K.R. (2006). "Merging Energy-Based Design Criteria and Reliability-Based Methods: Exploring a New Concept", Earthquake Engineering & Structural Dynamics, Vol. 35, No. 13, pp. 1677–1698.
9. Goel, R.K. and Chopra, A.K. (2004). "Evaluation of Modal and FEMA Pushover Analyses: SAC Buildings", Earthquake Spectra, Vol. 20, No. 1, pp. 225–254.
10. Gupta, A. and Krawinkler, H. (1999). "Seismic Demands for Performance Evaluation of Steel Moment Resisting Frame Structures", Technical Report 132, John A. Blume Earthquake Engineering Center, Stanford University, Stanford, U.S.A.
11. ICC (2006). "International Building Code", International Code Council, Washington, DC, U.S.A.
12. Manfredi, G. (2001). "Evaluation of Seismic Energy Demand", Earthquake Engineering & Structural Dynamics, Vol. 30, No. 4, pp. 485–499.
13. Prakash, V., Powell, G.H. and Campbell, S.D. (1993). "DRAIN-2DX Base Program Description and User Guide: Version 1.10", Report UCB/SEMM-1993/17, Department of Civil Engineering, University of California, Berkeley, U.S.A.
14. Prasanth, T., Ghosh, S. and Collins, K.R. (2008). "Estimation of Hysteretic Energy Demand Using Concepts of Modal Pushover Analysis", Earthquake Engineering & Structural Dynamics, Vol. 37, No. 6, pp. 975–990.
15. Roy Chowdhury, A. (2008). "MPA-Based Estimation of Hysteretic Energy Demand—$P-\Delta$ Effects and Buildings with Plan-Asymmetry", M.Tech. Thesis, Department of Civil Engineering, Indian Institute of Technology Bombay, Mumbai.
16. Zahrah, T.F. and Hall, W.J. (1984). "Earthquake Energy Absorption in SDOF Structures", Journal of Structural Engineering, ASCE, Vol. 110, No. 8, pp. 1757–1772.

ISET Journal of Earthquake Technology, Paper No. 512, Vol. 47, No. 2-4, June-Dec. 2010, pp. 87–108

30th ISET Annual Lecture

EVOLUTION OF SEISMIC DESIGN OF STRUCTURES, SYSTEMS AND COMPONENTS OF NUCLEAR POWER PLANTS

K.V. Subramanian
Tata Consulting Engineers Limited
Mumbai

ABSTRACT

Safety of the personnel of a nuclear power plant (NPP) and the environment around the plant should be ensured against all natural hazards including earthquakes. With public safety as the paramount concern, NPP facilities are designed to withstand low-probability, high-magnitude earthquakes. In this paper, details are discussed regarding the evolution of seismic analysis and design aspects of nuclear power plant structures, systems and components.

KEYWORDS: Nuclear Power Plant, Seismic Analysis, Design of SSCs, Retrofitting

INTRODUCTION

The constituent systems of nuclear power plants (NPPs), known as SSCs, are broadly classified into structures, systems (i.e., piping, electrical, control and instrumentation) and components with unique characteristics of their own. The structures, systems and components of an NPP need to be designed for normal operating loads such as dead weight, weight of supporting systems and components, pressure, temperature, normal operating vibratory loads, and accidental loads caused due to both external and internal events. The severity of external events is site-specific and depends on the site where the facility is proposed to be set up. To ensure adequate safety of the facility, an appropriate site determined by the siting criteria of NPPs needs to be selected. This site has to be examined with respect to the frequency and severity of natural phenomena and man-induced events. One of the accidental natural phenomena is earthquake.

NPPs in India have their origin in the setting up of two boiling water reactors by General Electric in 1969. This was followed by the growth of NPPs in India with the CANDU pressurized heavy water reactors (PHWRs) of Atomic Energy of Canada Limited, Canada set up in 1973. The evolution of seismic design criteria had its beginning in the development of the indigenous nuclear programme.

The recognition of seismic design requirements for NPPs other than those defined in various codes began in the late 1960s. The early plants designed, for example in U.S.A., had no seismic requirements. With the exception of active seismic regions, the resultant lateral seismic loads were less than the applicable lateral wind loads and would thus have little or no consequence on the design of engineered industrial facilities.

The safety considerations under earthquake loading with regard to nuclear facilities and the requirement of appropriate seismic investigation were not recognized in the plants set up in late 60's in India. The designs were performed by considering normal building codes and by arbitrarily increasing for NPPs the applicable seismic coefficients for the sites. The siting of plants in seismically prone regions (e.g., Narora) led to the development of specific seismic design criteria for nuclear power plants. These procedures became rigorous as regulatory requirements evolved. The development and current status with respect to seismic inputs, analysis and design of structures, systems and components are traced in this article.

GROUND MOTION

The possibility of earthquake damage to a NPP facility in contrast to a fossil fuel power facility constitutes a special safety problem due to the possibility of release of fission products. An uncontrolled release to the atmosphere would constitute a very serious hazard to human life in the immediate vicinity of the reactor and could lead to a serious biological hazard over a large area over a considerable period. Earthquakes are thus low-probability high-risk events.

The recognition of the need to have nuclear structures and systems designed for higher levels than specified by Indian codes began with Madras Atomic Power Station. The seismic design basis for this was taken as the lateral load coefficient of 0.1*g* against the horizontal coefficient of 0.02*g* as per IS-1893 for Zone II. The post-Koyna revision of the IS-1893 code and the siting of NPPs in seismically prone regions led to the introduction of an importance factor of 6 for the preliminary design of NPP structures in BIS (1975). The design of Dhruva Research Reactor was based on this approach. All NPPs since the Narora Atomic Power Station have been designed by using the site-specific ground motion criteria.

ESTABLISHMENT OF SITE-SPECIFIC GROUND MOTION

1. Deterministic Basis

1.1 Geological Investigations

To ensure the safety of a plant, detailed seismological and geological studies need to be performed considering the aspects such as capable faults, frequencies of earthquakes of different magnitudes (i.e., seismic activity), slope instability, liquefaction potential. An area of a circle of 300 km radius around the site is considered for investigation.

Geological investigations help in knowing the tectonic setting of the region, to arrive at the maximum earthquake potential associated with each active tectonic feature and to postulate the design basis events. Lineaments/faults are identified and studied particularly with respect to topography and geomorphology to find evidences of recent ground displacements and to ascertain their age and continuity. The faults are studied for assessing the seismic activities and identifying the various capable faults. Local tectonics, structural relationships of various faults, and correlations with historical earthquakes are studied.

1.2 Investigations of Past Earthquakes

All historical and instrumental earthquake data is collected. This primarily includes the data on magnitude or intensity, epicenter, depth of focus, duration of strong motion, and velocity and zone of influence depicted in isoseismic maps. This data helps in assessing the magnitudes and locations of possible earthquakes in the region.

1.3 Evaluation of Design Basis Ground Motion

The design basis ground motion at a site is given in terms of (i) peak ground acceleration and response spectral shapes for various values of damping, and (ii) time history of free-field acceleration in the horizontal and vertical directions. Based on the safety criteria, the systems of NPP are required to be designed for the S1 and S2 earthquakes in accordance with the national standards.

S1 Earthquake: This corresponds to the level of ground motion that can be reasonably expected to be experienced at the site area during the operating life of the plant. This is also referred to as the operating basis earthquake (OBE).

S2 Earthquake: This corresponds to the level of ground motion that has a very low probability of being exceeded and has a return period of the order of 10,000 years. This is referred to as the safe shutdown earthquake (SSE). All NPPs have to be designed such that, if a safe shutdown earthquake occurs, certain structures, systems and components remain functional to ensure the following:

- integrity of the reactor coolant boundary;
- capability to shut down the reactor and maintain it in safe shutdown condition; and
- capability to prevent or mitigate consequences or accidents resulting in an off-site exposure.

For an S2 level earthquake, conservatism in design is ensured by first postulating the occurrence of the potentially largest earthquake at the nearest point to the site on the seismically active structure or at the border of the seismo-tectonic provinces located within a tectonic zone of 300 km and then by estimating the peak ground acceleration to be produced at the site. Due consideration is given to the induced seismicity resulting from large dams/reservoirs or from extensive fluid injection/extraction from the ground.

The peak ground acceleration for a S1 earthquake is derived on the basis of historical earthquakes that have affected the site area. This has a low probability of being exceeded during the operating life of the plant. This has generally been defined as minimum one-half of that for SSE and under this event the plant is intended to remain in operation. However, an inspection is necessary on the seismic disturbance crossing the threshold value. This has become a utility and economic criterion, and the peak ground acceleration for OBE is sometimes lowered to one-third of that for SSE. Such a reduction, while reducing the plant cost, results in more frequent requirement of inspection and thus increased shutdown time.

In the absence of adequate strong-motion time histories obtained from the site, data collected from places having similar seismic and geological characteristics may be used. The confidence level of the specified response spectral shape should be conservatively high. This approach has been used in defining the site-specific inputs for the plants in India. In mid-80s, the concept of design standardization for the plants to be installed at the sites having similar seismological and geological conditions originated. Under this concept and based on the steps explained above, design inputs can be evolved and an envelope of the same that suits all the sites can be used for the design. One typical envelope design response spectrum for 7% damping, which meets the site requirements of Tarapur in Maharashtra, Kakrapar in Gujarat and Nagarjunasagar in Andhra Pradesh, was developed as shown in Figure 1. A response spectrum-compatible time history for this spectrum is shown in Figure 2.

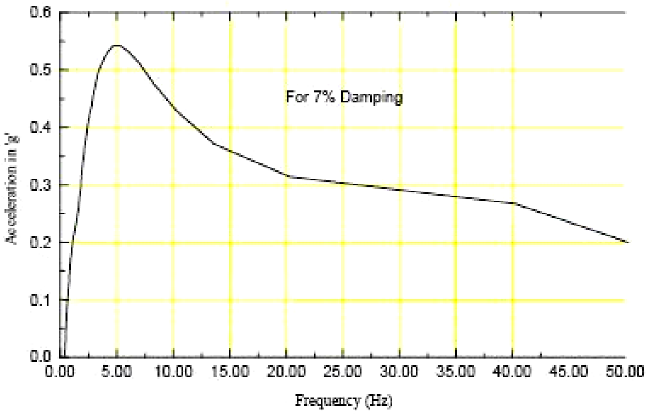

Fig. 1 Typical envelope design response spectrum for 7% damping

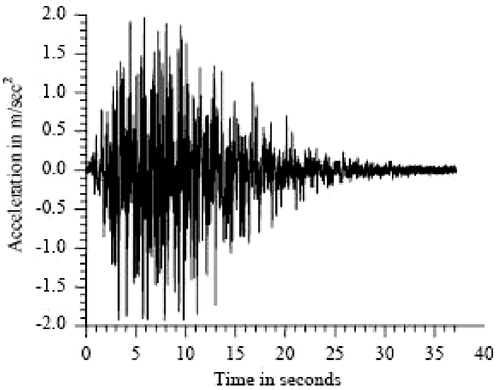

Fig. 2 Typical envelope design response spectrum-compatible time history

2. Uniform Hazard Spectra and Performance-Based Spectra

Internationally, it is recommended to adopt uniform hazard response spectrum (UHRS) and performance-based, site-specific, earthquake ground motions for a rational and graded approach to the design of SSCs of nuclear facilities. A probabilistic seismic hazard assessment (PSHA) provides an evaluation of the SSE recurrence during the design lifetime of the given facility, given the recurrence interval and recurrence pattern of earthquakes in the pertinent seismic sources. Within the framework of probabilistic analysis, uncertainties in the characterization of seismic sources and ground motions are identified and incorporated in the procedure at each step in the determination of SSE. This is now in place as an approach in USNRC regulatory guide 1.208 (USNRC, 2007a). UHRS involves following steps:

i) Carry out site- and region-specific geological, seismological, geophysical, and geotechnical investigations and develop an up-to-date site-specific database that supports site characterization and PSHA.
ii) Conduct probabilistic hazard analysis.
iii) Carry out probabilistic seismic hazard assessment.
iv) Develop UHRS for the annual exceedance frequencies of 1×10^{-4}, 1×10^{-5} and 1×10^{-6} at minimum of 30 structural frequencies approximately equally spaced on logarithmic frequency axis between 0.1 and 100 Hz.
v) Deaggregate mean probabilistic hazard characterization at the above annual frequencies.

The use of UHRS approach requires the availability of earthquake occurrence information associated with the known tectonic structures. Further, sufficiently large data samples need to be available. Efforts are now on to collect such information in the context of the Indian sub-continent. Work has been completed for a few sites such as Mumbai, Tarapur, and Kalpakkam. More work is to be carried out in order to develop confidence for adopting this procedure in NPP designs. A typical comparison of the UHRS and performance-based ground motion response spectrum as given in USNRC (2007a) is given in Figure 3.

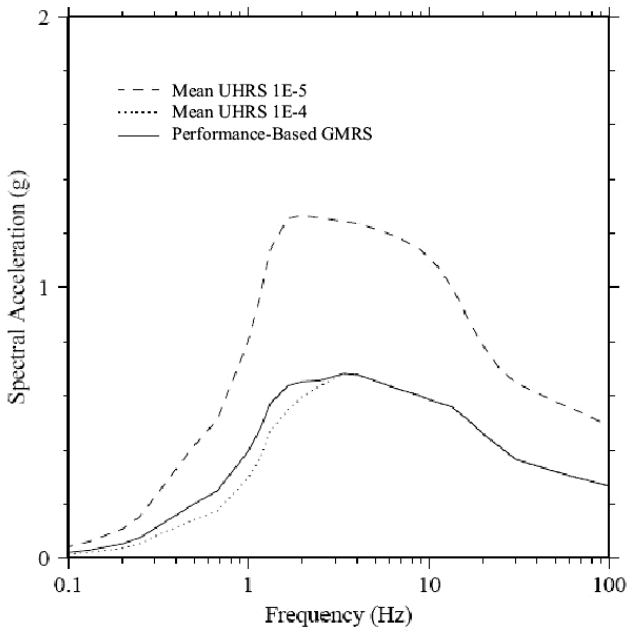

Fig. 3 Comparison of the mean 1×10^{-4} and 1×10^{-5} uniform hazard response spectra and the performance-based ground motion response spectrum

3. Tsunamis

With the occurrence of the great Indian Ocean tsunami on December 26, 2004, which had a pronounced effect on the eastern coast of India, suitable criteria are now in place in the regulatory standards of India. This has led to the development of a BIS standard for tsunami resistant design for buildings and structures. These criteria will also be introduced appropriately for NPP design.

EARTHQUAKE ANALYSIS

Indian standard code, IS 1893 (BIS, 2002), does not cover the earthquake-resistant design of nuclear structures. Hence, international standards, such as ASCE 4-1998 standard (ASCE, 2000), and various

USNRC regulatory guides and ASME codes are adopted for the analysis and design of NPP structures. Nevertheless, a code relevant in the Indian context is currently under publication by Atomic Energy Regulatory Board (AERB).

The equilibrium equations for a structure may be written in the following form:

$$[M]\{\ddot{u}\}+[C]\{\dot{u}\}+[K]\{u\}=-[M]\{1\}\ddot{u}_g \tag{1}$$

where $[M]$ is the mass matrix of the structure, $[C]$ is the damping matrix of the structure along with the supporting soil, $[K]$ is the stiffness matrix of the structure along with the supporting soil, and $\{1\}$ is the influence vector.

The coupled set of equations given in Equation (1) is solved simultaneously by using a numerical technique (Bathe and Wilson, 1976). The other approach is to de-couple the equations by using a modal transformation. This leads to equations at the modal level that can be solved independently. Such a transformation uses eigenvectors and eigenvalues, which represent the mode shapes and circular frequencies squared for the system, respectively. However, the analysis is generally carried out by using the standard commercial finite element (FE) packages, such as COSMOS, NISA, and ANSYS.

For accurate response predictions in SSCs subjected to the design ground motions derived as explained above, the inertia, stiffness and damping matrices of the SSCs need to be modeled appropriately. Some of the details of these parameters with regard to SSCs are explained below.

MATHEMATICAL MODELING OF STRUCTURAL SYSTEMS

Once the design input has been obtained, the next step is to collect the geometrical, material, loading and supports information of SSCs. With the help of this data along with the design earthquake input, analysis is performed to obtain the induced forces or stresses in the SSCs. The first step of analysis is modeling.

The mathematical model of the system should adequately represent the dynamic characteristics of the physical system, e.g., mass, stiffness and damping. For reactor building structures, stick models have been in vogue and have been refined over the years. The reactor buildings in Narora, for example, have been analyzed by using 2-D stick models. Certain structures and systems like Calandria end shield assembly have been included in coupled 2-D models. A refined approach using a 3-D stick model with the coupling of certain systems, as adopted in Tarapur for the 500 MWe PHWR, is briefly described here.

The nuclear containment structure and the model considered for the 500 MWe PHWR at Tarapur are shown in Figure 4. The containment structure consists of the internal structure (INTS) and calandria vault (CV) contained in the coaxial inner and outer containment walls (ICW and OCW) and cast monolithically with a circular raft. The OCW consists of a cylindrical reinforced concrete wall that has the diameter of 54.72 m and supports a reinforced concrete torispherical dome. The ICW consists of a prestressed cylindrical reinforced concrete wall that has the inner diameter of 49.5 m and supports a prestressed concrete torispherical dome. The INTS supports fuelling machines, steam generators, pumps, pressuriser, a large number of piping systems, etc. The CV supports the calandria end-shield assembly, reactor control devices, etc.

For evaluating seismic response, the model considered should represent the structure as accurately as possible. The finite element method has been most popular in modeling structures for seismic analysis. There is no difficulty in modeling a frame-type structure. However, the modeling of a containment structure with complex geometry and made of shear walls, beams, columns and floors is not straight-forward.

A containment structure can be modeled accurately either by plate/shell or by 3-D brick elements. However, the analysis may be very cumbersome and time-consuming. This also requires large memory and high-speed computing facilities. If the stiffness variation is large in the structure, there could be numerical problems. To avoid these problems, beam models are normally used for obtaining the global seismic response. These are finally applied on the 3-D finite element model for evaluating the design stresses.

1. Modeling of Structural Stiffness

1.1 Beam Model

There are, in principle, two techniques to evaluate the stiffness of a beam model: (i) the conventional 2-D beam model technique; and (ii) the 3-D beam model technique based on strain-energy equivalence. These techniques are explained below.

Conventional 2-D Beam Model Technique: This is commonly used where the shear centers of various structural sections lie on the centerline of the building. Moreover, it is assumed that the structure behaves like a beam, and classical beam assumptions are valid. The mass of the structure is lumped at a series of nodes at the center of the building. The beam-section properties, such as cross-sectional area, shear area, moment of inertia, are calculated by using the classical formulae. These properties are then used for calculating the stiffness of the member. The effects of the flexibility of slabs, offset, partial support, etc., are neglected. The properties for containments and raft are also calculated by using the classical formulae (Reddy et al., 1996).

3-D Beam Model Technique Based on Strain-Energy Equivalence: In this method, the structure is modeled by using 3-D beam properties derived based on the strain-energy equivalence between 3-D finite element model and 3-D beam model (Reddy et al., 1997). Unlike the above method, lateral torsional coupling and the effect of flexibility in floors, offset and partial support of walls is accounted for. In this method, the beams are located at the shear center.

1.2 3-D Model

In the case of structural systems, which are integrated and connected, the stick-model approaches are not feasible. A 3-D finite element model becomes the appropriate option, with high-capacity computing options being available.

The nuclear island connected building (NICB) of PFBR is a large reinforced concrete building of size 92.6×83.2 m in plan as shown in Figure 5(a). It consists of a centrally located reactor containment building, which is surrounded by seven buildings, connected monolithically with each other and supported on a common base raft of size 101.80×92.4 m. The resisting system of the structure consists of shear walls and frames made of beams and columns. The response of the structure to various static and seismic conditions is evaluated by considering the effects due to soil-structure interaction, coupled and decoupled secondary systems, and fluid-structure interaction. Figure 5(a) gives a 3-D view and the plans of the structure. Figure 5(b) depicts the 3-D finite element model. Tables 1 and 3 indicate a few fundamental frequencies of the structural system.

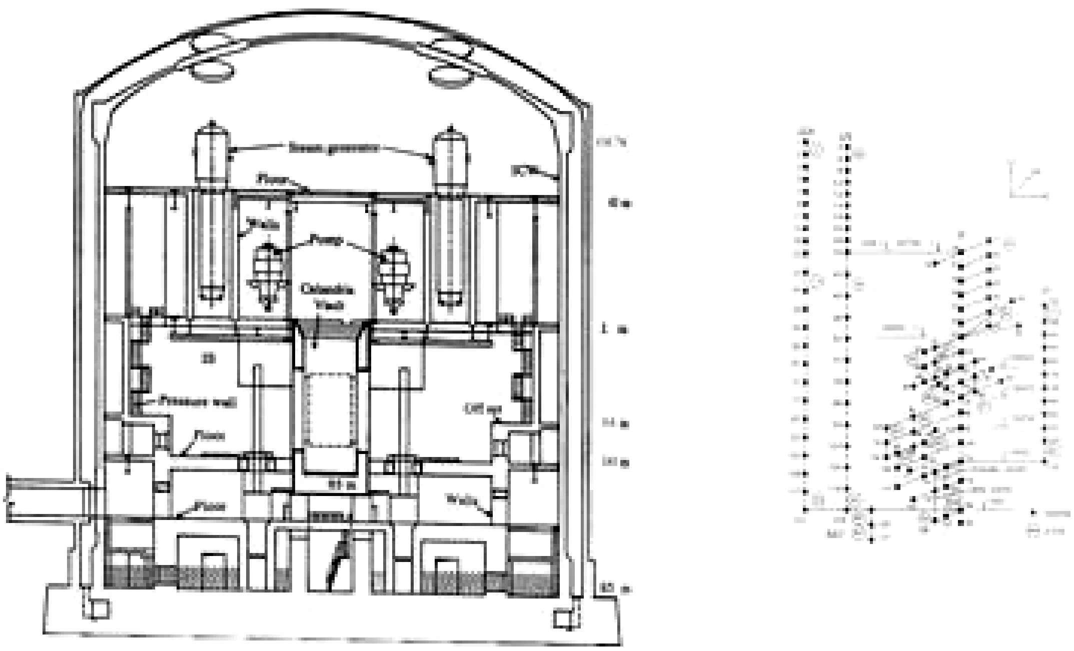

Fig. 4 500 MWe PHWR containment structure and 3-D beam model

Table 1: Comparison of Frequencies and Participation Factors of Reactor Building

Mode	3-D FEM Model		Beam Model			
			Strain Energy Based		Conventional	
	Frequency (Hz)	Participation Factor	Frequency	Participation Factor	Frequency	Participation Factor
1	3.70 (E-W)	41.38	3.73	43.76	5.45	41.63
2	3.87 (N-S)	36.74	4.03	40.26	5.46	40.90
3	9.27 (Vertical)	25.00	9.75	34.42	12.69	35.41

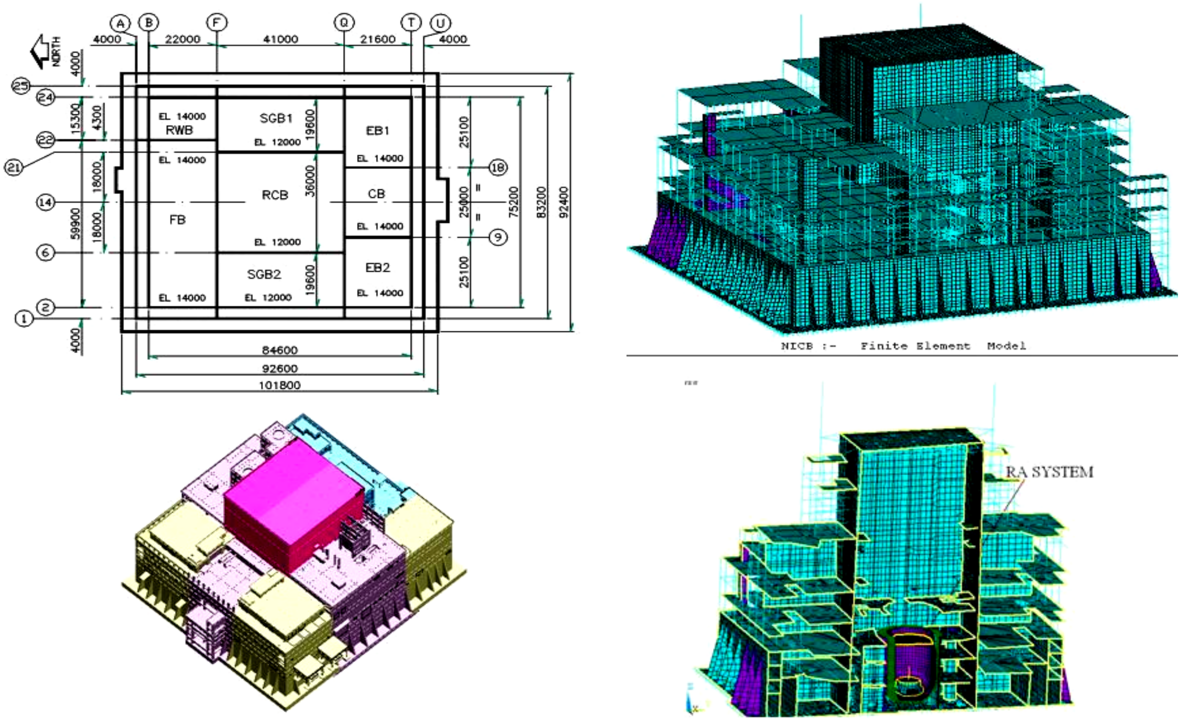

(a) (b)

Fig. 5 Nuclear island connected building of PFBR: (a) 3-D view and plan, (b) 3-D finite element model with 120,000 nodes and 725,000 degrees of freedom

2. Modeling of Structural Mass

The exact formulation of the dynamic response of a structure involves an infinite number of degrees of freedom. For most structures, however, the response may be adequately described via a limited number of discrete points (or joints) within the system. In the NICB of PFBR, the mass and mass moment of inertia are lumped at each floor level and at certain intermediate points, where the cross-section is changing. The mass and mass moment of inertia values are calculated about the mass centers. The mass at each floor node is calculated by summing the individual masses of slab, mass of equipment, etc. and 50% of the live load on slab area. The mass due to the self-weight of the sections of OCW, ICW, INTS, CV and raft are calculated between two connecting nodes and distributed equally to those nodes.

Table 1 shows the comparison of the frequencies and participation factors of the conventional beam model technique and beam model technique based on strain-energy equivalence with those of the 3-D finite element model. It can be seen that the beam model technique based on strain-energy equivalence calculates frequencies close to those of the 3-D finite element model and is generally recommended for the seismic analysis of reactor building. The same methodology has been extended to the advanced heavy water reactor (AHWR) building, and analysis was performed by using the models shown in Figure 6. Such approaches are amenable to the structural systems founded on independent foundations and not connected to each other in the superstructure. Figure 7 shows the development of the mass participation across different modes.

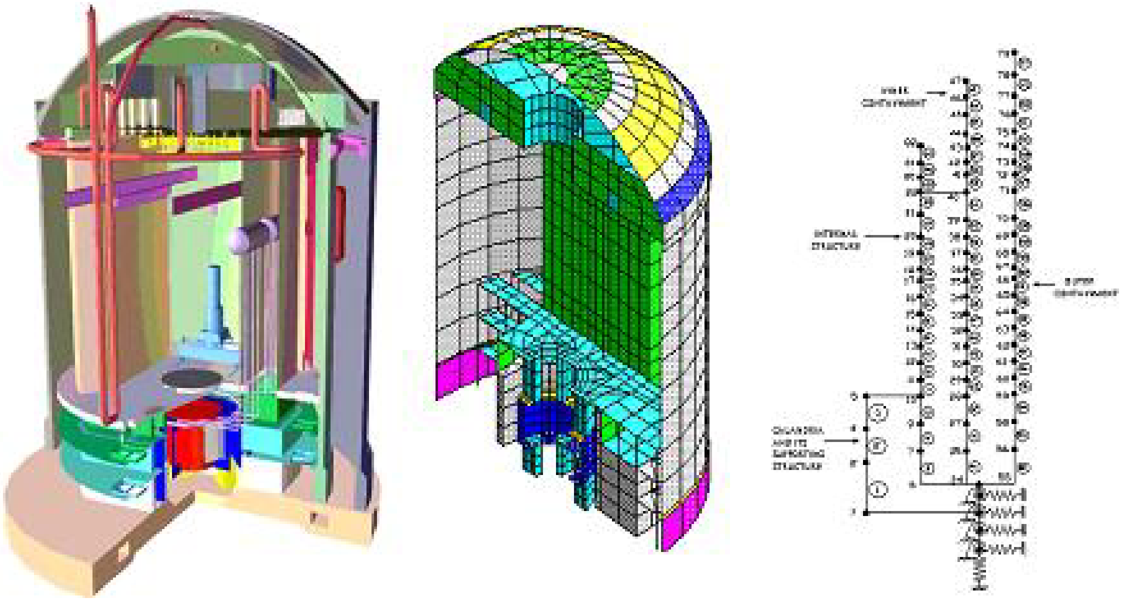

Fig. 6 AHWR containment structure: 3-D model and beam model

3. Soil-Structure Interaction (SSI)

When a structure vibrates under the action of an earthquake, the ground has an effect on the response of the structure, and at the same time the structure has an influence on the ground on which the structure is supported. The structure and ground interact with other during the earthquake. This phenomenon is referred to as soil-structure interaction. This may be separated into two types: kinematic interaction and inertial interaction. The kinematic interaction is the phenomenon that the rigid foundation constrains and averages the ground motion when seismic waves impinge on the foundation. The inertial interaction is the phenomenon that the inertial forces generated in the structure give rise to a new ground motion in the soil, when those forces are transmitted to the ground.

The soil-structure interaction effects are significant not only in evaluating the seismic response of structures but also in the assessment of structural safety against earthquakes. In the analysis of a soil-structure system, one is obliged to introduce many simplifications, idealizations, and/or assumptions not only in making the mathematical models of structures but also in their numerical evaluation. Most of these assumptions are concerned with soil because of the uncertainty of its properties as listed in Table 2.

While a variety of computational procedures to analyze the impedance functions and foundation input motions are available, an appropriate procedure can be chosen according to the purpose. The analysis procedures are based on using the available numerical evaluation procedures after suitable approximations or discretizations are introduced. A classification of these procedures is given in Table 4.

Table 2: Assumptions in Making Mathematical Model and Numerical Calculations

Issue	Assumed Items
Soil	• Idealization of soil medium • Homogeneous or horizontal stratum • Type of damping • Soil constraints
Interface	• Perfect bonding
Numerical Calculations	• 2-D, pseudo 3-D analyses • Discretization of soil medium or interface • Artificial boundary when FEM is used • Equivalent linearization of non-linear soil

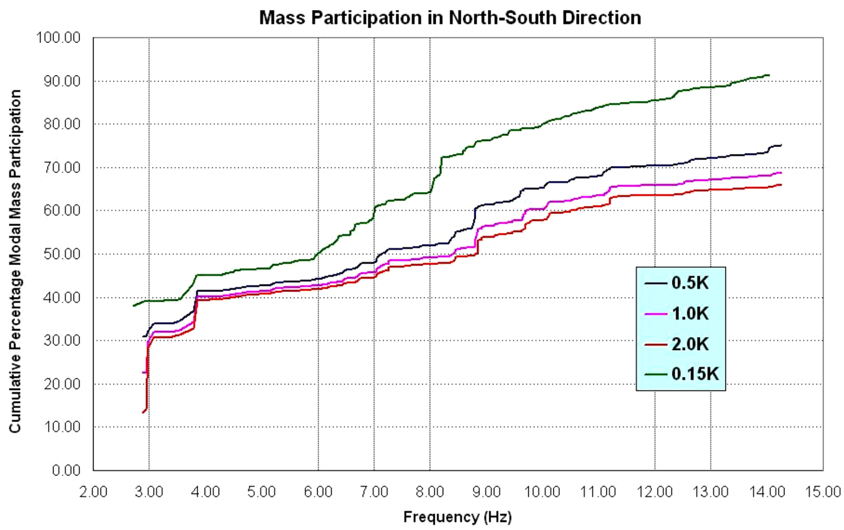

Fig. 7 Mass participation in the North direction for various values of sub-grade reaction

Table 3: Results of Frequency Analysis with 1.0 K Sub-grade Stiffness

S. No.	North-South Direction		East-West Direction		Vertical Direction	
	Frequency (Hz)	% Modal Mass	Frequency (Hz)	% Modal Mass	Frequency (Hz)	% Modal Mass
1	2.92	22.48	2.95	2.30	6.09	1.00
2	2.98	6.96	3.12	14.71	7.33	2.10
3	3.12	3.15	3.47	14.53	7.71	1.43

Table 4: Classification of Analysis Procedures (Soil-Structure Interaction)

Analysis Procedures	**Analytical**	• Exact
	Discrete Methods	• Finite element method • Finite difference method • Lumped mass model
	Others	• Baranov Novak method

A rational evaluation of soil-structure interaction effects during the postulated earthquake events is of prime importance in various analyses of NPPs. The soil-structure interaction can alter the frequencies of vibration of the structure and it can also affect the stresses and displacements in various components of the structure.

For rigid foundations where the super-structure is idealized as a stick model and the base foundation is represented as a single lumped-mass parameter system, the spring and damping coefficients obtained via impedance-function formulations and available in ASCE 4-1998 standard (ASCE, 2000) are used for representing the translational and rotational springs.

For distributed finite element models like the NICB structure, to simulate soil-structure interaction in the domain of dynamic loading, the base raft is incorporated in the global finite element model by using an assemblage of shell elements that interacts with the foundation base medium at all points of contact. In this case, the extension of the above method for raft foundation, as detailed in Arya et al. (1979), is adopted.

The vertical and horizontal springs based on impedance-function formulations are idealized at all nodes of raft. The vertical springs are distributed in plan and those resist the rocking motions about the N-S and E-W axes besides offering vertical stiffness. The horizontal springs resist the torsional motion of the structure besides offering horizontal stiffness. For idealizing these tension-compression springs, a spar element is used, which is a three-dimensional, uniaxial, tension-compression element with three degrees of freedom at each node. Damping is specified for every discrete nodal spring in the form of damping expressed as a percentage of critical damping.

4. Modeling of Systems and Components

For the seismic analysis of piping and equipments, generally finite element method is used. In this method, the stiffness, mass and damping are modeled appropriately and one of the following techniques is adopted.

4.1 Rigid Body Model

For this model, the item itself is assumed rigid (i.e., the fundamental frequency is assumed to be larger than the typically accepted limit of 30 Hz). The model is typically represented as a rigid body with attachment at the support points represented by springs or stiffness/flexibility matrices. The response of the item then would be by rocking or translational modes of vibration at the support points. Typical valves, pumps, motors, fans, and some heat exchangers fall in this category.

4.2 Single Mass Model

In this model, the total mass is assumed to be lumped at a single point, with composite stiffness restraining the mass represented as a single element. More than one degree of freedom may be permitted. In general, this modeling is considered as an alternative to the above method and is applied to the same type of systems.

4.3 Beam Model or One-Dimensional Finite Element Model

This modeling is typically applied to beams, columns, frames, ducts, cable trays, conduits, tanks, cabinets, storage racks, pressure vessels and heat exchangers, and is expressed as a continuous or one-dimensional finite element in a two- or three-dimensional space. The masses are represented by lumped parameters, which develop a diagonalized elemental mass matrix, or by means of consistent mass matrices, which have the same off-diagonal form as the elemental stiffness or flexibility matrices.

4.4 Plate/Shell or Two-Dimensional Finite Element

This type of modeling is adopted for those items whose primary mode of failure is via biaxial bending stress, plane stress or plane strain. Typically included in this category are cabinets, tanks, pressure vessels, and heat exchangers whose shells support significant out-of-plane loads, which would tend to excite shell or local modes of vibration.

4.5 Beam Model Based on Energy of Plate/Shell Finite Element

For the equipments, which have sections of irregular shapes, beam models of the equipments are generated by using energy equivalence between the plate/shell finite element and beam models.

4.6 Three-Dimensional Finite Element

This type of modeling is expensive and is thus preferable for local analyses to obtain correct stress picture at openings, nozzle junctions, etc.

4.7 Piping Models

Straight pipe element and/or pipe bends are used for modeling piping and supports, valves, etc., which are modeled with the above methods.

5. Supports for Piping Systems

Piping systems are supported on conventional supports, such as spring hangers, restraints, guides, and seismic supports called snubbers.

5.1 Spring Hangers

A spring hanger, as shown in Figure 8(a), is used for the piping carrying high-temperature fluid/steam in order to enable a free (axial and lateral) thermal expansion of the piping.

5.2 Rigid Restraints

A rigid restraint, as shown in Figure 8(b), is used where no thermal expansion-related movement of the pipe/equipment is expected along the support direction. Dead weight, thermal loads and service loads can be supported by these restraints. In these types of supports, a limited amount of energy associated with the oscillatory motion is dissipated due to the rubbing or frictional movements at the hinge joints. The type of hinge joint dictates the actual amount of energy dissipation. The spherical ball and groove type of hinge joint is found to be more effective in dissipating the energy. However, the force-displacement characteristics are highly nonlinear and the amount of energy dissipation is very small.

5.3 Pipe Guides

Pipe guides and sliding supports, as shown in Figure 9, were originally used for the piping/equipment to allow free thermal expansion movement. Recently, it has been found that these supports have an inherent characteristic to absorb energy due to the oscillatory motion. In order to have free thermal expansion, the coefficient of friction between the pipe and the support should be small and should be maintained through out the service of the piping system. To maintain a constant coefficient of friction, there should not be any corrosion on the surface of the pipe or the support. To avoid corrosion problems, materials, such as Teflon, Ferro asbestos sheets, are used. A high coefficient of friction may be good for high-energy dissipation, but on the contrary, it will result in more thermal stresses in the piping/ equipment. Due to this problem, materials with low coefficients of friction are being used.

5.4 Snubbers

Snubbers, which are generally called seismic anchors, are of two types—mechanical snubbers and hydraulic snubbers.

Mechanical Snubber: A mechanical snubber, as shown in Figure 10, consists of a ball screw that converts the linear motion of piping/equipment into the rotary motion of the flywheel attached to the end of the ball screw shaft. The flywheel additionally has a breaking mechanism, which restrains the movement of the piping/equipment above certain earthquake acceleration level but allows free movement under normal operation. Snubbers do not take any sustained loads.

Hydraulic Snubber: A hydraulic snubber consists of an orifice, a moving piston and a cylindrical casing filled with operating oil. The piston is connected to the piping/equipment through the connecting rod and cylinder is connected to the building structure. In the case of thermal expansion movement, which is slow and gradual, the operating oil moves through the orifice, enabling the piston to move almost with no resistance from the hydraulic pressure. On the other hand, when a rapid seismic motion occurs, the orifice is shut by the hydraulic pressure (as high resistance is offered by the orifice to the large flow rate of the oil required for the rapid movement of piston), preventing the flow of operating oil. This results in the suppression of piping/equipment movement.

5.5 Limitations of Conventional Support

The conventional supports except snubbers can act either as restraints or allow free motion and cannot thus serve both purposes of allowing free motion during the normal operations and restraining or energy dissipation during an earthquake. However, utilities have strong incentives to remove snubbers from operating NPPs and are avoided in new plants due to the following reasons:

a) It is expensive to maintain snubbers since they require periodic testing to ensure meeting stringent functionality specifications. On average, the maintenance cost of a single snubber is estimated at \$2000 per year. For qualified snubbers, repairs or replacements could incur an additional cost.
b) The structure of snubber is complex; it provides less damping and is expensive. In addition to this, the mechanical snubber may pose locking problem and the hydraulic snubber, if used, may leak and may not work when required.
c) Snubbers congest the working space and thus impede in service inspection.
d) An inadvertent snubber lock-up in a mechanical snubber can induce higher thermal stresses during normal operations, which is undesirable from the viewpoint of piping fatigue.

In order to overcome the above difficulties, modern damping devices called seismic response control devices have been developed fulfilling the following requirements:

- high-damping ability for any dynamic impact (e.g., due to vibration, shock, and seismic effects);
- long service life without repairing;

- radioactive and thermal resistance;
- negligible reaction force to the system under thermal expansion;
- lack of time delay under dynamic loads;
- ability to sustain overloading without losing functionality and integrity;
- ability to regulate damping necessary for the system; and
- low primary, inspection and maintenance cost.

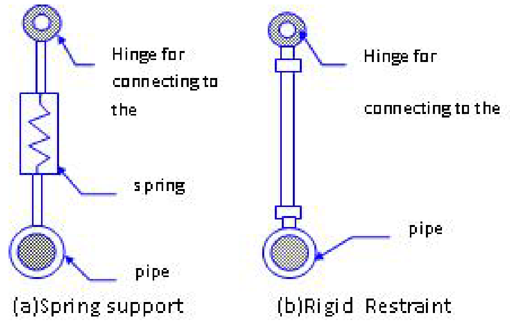

Fig. 8 Spring and rigid restraints

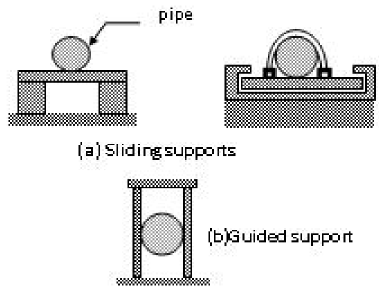

Fig. 9 Pipe guides

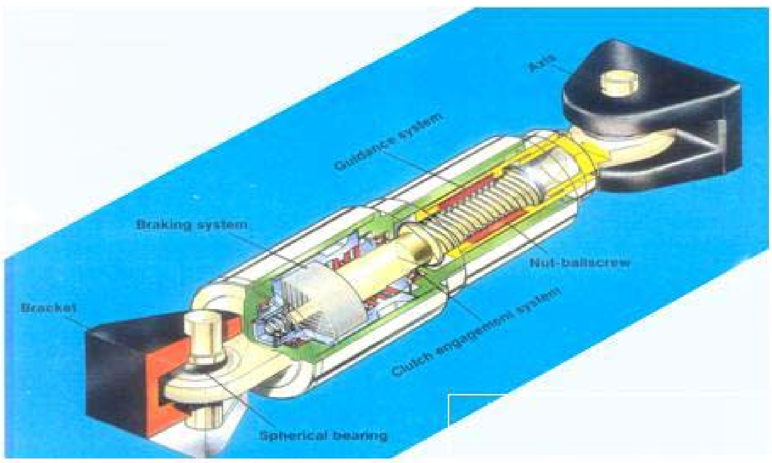

Fig. 10 Mechanical snubber

6. Structure-Equipment Interaction

The internal structure of a reactor building supports equipments and piping systems. The equipments may interact with the structure during an earthquake. This results in variations in the uncoupled response, wherein the uncoupled response is calculated for the equipments and structure separately. The best way of accounting for the interaction effects of the structure and equipments is by coupling those together and analyzing for the given earthquake load. However, due to practical reasons, it is not preferred. In fact, the equipments that significantly affect the uncoupled natural frequencies of the structure/equipments are identified by using the decoupling criteria (ASCE, 2000; USNRC, 1989) as given below:

- Decoupling can be done for any R_f, if $R_m < 0.01$, where R_f is the ratio of the frequency or modal frequency of the uncoupled equipment to that of the uncoupled structure and R_m is the ratio of mass or modal mass of the uncoupled equipment to that of the uncoupled structure. Dominant modes (with > 20% mass participation) only are considered for calculating the frequency and mass ratios.
- If $0.01 \leq R_m \leq 0.1$, decoupling can be done, provided $0.8 \geq R_f \geq 1.25$.
- If $R_m > 0.1$, an approximate model of the secondary system (e.g., equipment) should be included in the primary system (i.e., the supporting structure).
- For rigid equipment whose frequency is more than 33 Hz, only the mass of the equipment should be included.

This criterion is also represented graphically in Figure 11. If the frequency and mass ratio fall in the region "coupling is required", the corresponding equipment is coupled with reactor building and seismic analysis is performed.

The above criterion is not straightforward for applying to the complex structures, such as reactor containment structure. Modifications have been suggested (Reddy et al., 1994) that make the criterion applicable to the complex structures**.** The above criterion is also not applicable to the multi-connected equipments. A new criterion (Reddy et al., 1998) has been developed that can be used for checking the decoupling requirements of multi-connected equipments.

7. Damping

The damping values that can be used for SSCs, made of different materials and by using different construction and fabrication methods, are continuously updated with gain in knowledge from experiments on SSCs and the performance of SSCs under actual earthquakes. This has evolved following extensive studies and the current USNRC regulatory position as indicated in Table 5. A comparison of the old and new damping values for certain SSCs is indicated in this table. Additional details are available in USNRC regulatory guide 1.61 (USNRC, 2007b).

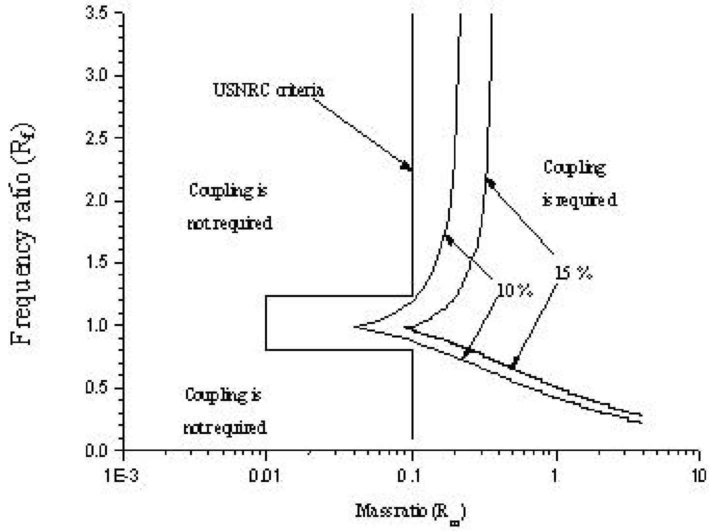

Fig. 11 Decoupling criteria for the equipment connected to the structure at single location

Table 5: Damping Values for Various Structures in Percentage of Critical Damping (USNRC, 2007b)

Structure Type	OBE		SSE	
	Old	New	Old	New
Pipe Diameter > 12"	2	3	3 (for OBE > 1/3 SSE)	4
Pipe Diameter < 12"	1		2	
Welded Steel Structure	2	3	4	4
Bolted Steel Structure	4	5	7	7
Pre-stressed Concrete	2	3	5	5
RCC	4	4	7	7
Reinforced Masonry	—	4	—	7

7.1 Piping

It is evident that in the case of piping systems, constant damping values presently prescribed by USNRC are higher than the earlier values for both response spectrum and time history analyses. As an alternative, for response spectrum analysis the envelope of the SSE or OBE response spectra at all support points and the frequency-dependent damping values, as shown in Figure 12, are accepted subject to the following restrictions:

a. If the damping values specified in USNRC regulatory guide 1.61 (USNRC, 2007b) are to be used for equipments other than piping, they should be used consistently.
b. The use of the specified damping values is limited to response spectral analyses.
c. When used for the reconciliation or support optimization of the existing designs, the effects of increased motion on existing clearances and online mounted equipments should be checked.
d. The frequency-dependent damping is not appropriate for analyzing the dynamic response of piping, while using the supports designed to dissipate energy by yielding.
e. The frequency-dependent damping is not applicable to the piping in which stress-corrosion cracking has occurred, unless a case-specific evaluation is provided, reviewed, and found acceptable by the NRC staff.

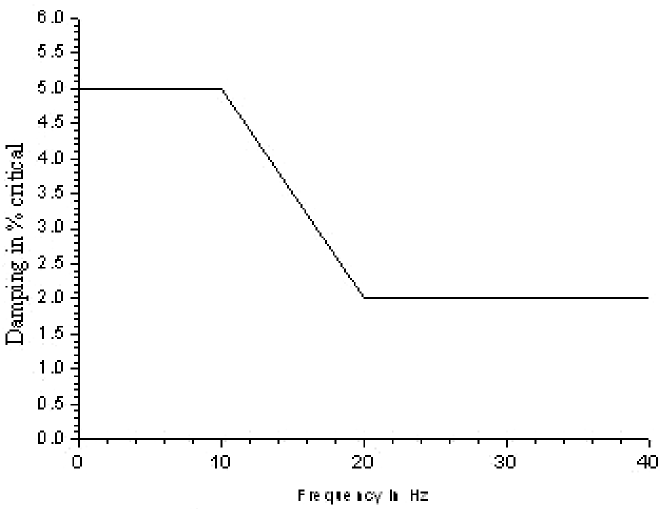

Frequency-Dependent damping

Fig. 12 Variation of damping with system frequency

7.2 Damping in Soil

The ASCE 4-1998 standard (ASCE, 2000) procedures for the evaluation of soil damping are adopted. For stick models, the damping of 7% is specified for the rocking mode. In the case of finite element models, the foundation stiffness is in a distributed form of vertical springs at each node of the base raft. These vertical springs resist the rocking motion. For the rocking mode, damping for the vertical springs is taken as 7%. The rocking mode of motion about the horizontal axis is excited due to the horizontal excitation. Hence, under the N-S and E-W excitations, damping for the vertical springs is specified as 7%.

Damping is evaluated by using the ASCE 4-1998 standard (ASCE, 2000) recommendations for the values over 30% in the vertical direction. However, this is restricted to 30% in the vertical direction. Though these provisions for damping are for a stick model, the same can be used for an individual vertical spring in the finite element model. The damping for a single spring-mass system based on $\left[K\right]$ and $\left[M\right]$ and given by impedance functions is adopted for the elemental springs used in the finite element analysis. These vertical springs do not come under the rocking mode under the vertical excitation. Hence, the damping is specified as 30% under the vertical excitation.

COMPUTATION OF RESPONSE

There are four popular methods, which can be used for the determination of seismic response:

(a) time-history method:
  - direct step-by-step integration technique,
  - modal superposition technique;

(b) response spectrum method;

(c) complex frequency response method; and
(d) equivalent static method.

In the above, method (c) deals with the frequency-domain analysis. This requires the power spectral density function (PSDF) of the ground motion to be specified. There are no well-defined and acceptable methods to obtain this. Hence, this method is not generally used. Method (d) can be adopted, where the seismic criteria will not control the design. Hence, out of these methods, methods (a) and (b) are most often used in the analysis of NPP systems. However, method (a) is used for response calculation as well as for floor response spectra generation, and method (b) is used only for response calculation. The floor response spectra generated are used for the design of equipment and piping after peak broadening and smoothening.

1. Number of Modes Considered in Modal Superposition Method or Response Spectrum Method

The system response evaluated is the combination of responses obtained in different modes. A sufficient number of modes should be selected to evaluate accurate response of the system. The number of modes included in the analysis should be sufficient to ensure that the inclusion of all remaining modes does not result in more than 10% increase in the total response of interest. However, the following two criteria are adopted, while choosing the minimum number of modes:

i. The number of modes extracted is such that the highest mode corresponds to a frequency greater than or equal to 33 Hz.
ii. The number of modes extracted is such that the cumulative modal mass is more than 90% in each of the three directions.

2. Combination of Modal Responses

Following modal combination rules have been in vogue as per the USNRC regulatory guide 1.92 (USNRC, 1976):

i. SRSS method,
ii. 10% method,
iii. double sum method, and
iv. grouping method.

For the combination of spatial components, procedures like SRSS combination and 100-40-40 method have been proposed and are in vogue. The procedures to evaluate the rigid-body response (or, the missing mass effect) are also adopted in the designs of all SSCs in NPPs. The current procedures formulated by AERB for Indian plants have adopted this criterion.

USNRC regulatory guide 1.92 (USNRC, 2006) has now adopted the following approaches, which could become the criteria adopted internationally.

i. SRSS method, and
ii. general modal combination rules:
    a) Rosenblueth correlation coefficient,
    b) Der Kiureghian correlation coefficient.

2.1 SRSS Rule for Well-Separated Modes

In a response spectrum-based modal dynamic analysis, if the modes are not closely spaced (two consecutive modes are defined as closely spaced if their frequencies differ from each other by 10% or less of the lower frequency), the representative maximum value of the particular response of interest for design should be obtained by taking the square root of the sum of the squares (SRSS) of the modal maxima of the same response. Mathematically, this can be expressed as

$$R = \left[\sum_{i=1}^{n} R_i^2 \right]^{1/2} \tag{2}$$

where R is the representative maximum value of the particular response of a given element to a given component of the earthquake ground motion, R_i is the peak value of the response of the element due to the ith mode, and n is the number of significant modes considered in the modal response combination.

USNRC regulatory guide 1.92 (USNRC, 2006) defines closely spaced frequencies as a function of critical damping ratio:

- For critical damping ratios ≤ 2%, modes are considered closely spaced if the frequencies are within 10% of each other (i.e., for $f_i < f_j$, $f_j \le 1.1\, f_i$).
- For critical damping ratios > 2%, modes are considered closely spaced if the frequencies are within five times the critical damping ratio of each other (i.e., for $f_i < f_j$ and 5% damping, $f_j \le 1.25\, f_i$; for $f_i < f_j$ and 10% damping, $f_j \le 1.5\, f_i$).

2.2 General Modal Combination Rule (Including Closely Spaced Modes)

A general modal combination rule considering closely spaced and well separated modes may be described as follows:

$$R = \left[\sum_{i=1}^{n} \sum_{j=1}^{n} \varepsilon_{ij} R_i R_j \right]^{1/2} \tag{3}$$

On substituting $\varepsilon_{ij} = 1.0$ for $i = j$ and $\varepsilon_{ij} = 0.0$ for $i \neq j$, this equation reduces to the SRSS combination rule. If the modes are closely spaced, SRSS rule is not applicable and one of the methods described below should be used.

Rosenblueth Correlation Coefficient: Rosenblueth has evolved following formula, based on the random vibration approach, for the representative maximum value, with coefficient ε_{ij} expressed as a function of modal frequencies and modal damping and the duration of strong motion t_d :

$$R = \left[\sum_{k=1}^{N} \sum_{s=1}^{N} \left| R_k R_s \right| \varepsilon_{ks} \right]^{1/2} \tag{4}$$

where

$$\varepsilon_{ks} = \left[1 + \left\{ \frac{(\omega_k' - \omega')}{\xi_k' \omega_k + \xi_s' \omega_s} \right\}^2 \right]^{-1} \tag{5}$$

with

$$\omega_k' = \omega_k \sqrt{1 - \xi_k^2} \tag{6}$$

$$\xi_k' = \xi_k + \frac{2}{t_d\, \omega_k} \tag{7}$$

and ω_k and ξ_k being the modal frequency and damping ratio, respectively, in the k th mode.

Der Kiureghian Correlation Coefficient: This method does not take into account the duration of the earthquake ground motion. It assumes the earthquake loading to be a white noise with infinite duration and the representative maximum value is expressed as

$$R = \left[\sum_{k=1}^{N} \sum_{s=1}^{N} R_k R_s \varepsilon_{ks} \right]^{1/2} \tag{8}$$

with

$$\varepsilon_{ks} = \frac{(\omega_k + \omega_s)^2 \xi^2}{(\omega_k - \omega_s)^2 + (\omega_k + \omega_s)^2 \xi^2} \tag{9}$$

for constant damping ratios and

$$\varepsilon_{ks} = \frac{2\sqrt{\xi_k \xi_s} \left[(\omega_k + \omega_s)^2 (\xi_k + \xi_j) + (\omega_k - \omega_s)^2 (\xi_k - \xi_j) \right]}{4(\omega_k^2 - \omega_s^2) + (\omega_k + \omega_s)^2 (\xi_k + \xi_j)^2} \tag{10}$$

for different damping ratios.

SEISMIC DESIGN OF SYSTEMS AND COMPONENTS

Generally various components and systems in an NPP are supported on the structure. Some of the large-size components may influence the behavior of structures supporting these components, and this influence is qualitatively checked by using the decoupling criterion indicated above as per the ASCE/ ASME specifications. This criterion is based on the frequency and mass ratios of the uncoupled component which determine whether the component will alter the vibration characteristics of the structure or not. If it is so, the coupled models of structures and components are generated and analyzed. The systems, such as piping, instrumentation and control, may not alter the structural vibration characteristics because those are light in nature. However, for the design of such systems and components, input motions are generated at the support locations in the structures. These motions become inputs for the qualification of such systems. These input motions are very easy to generate in the beam models, but in the case of 3-D models where there will be a large number of nodes at each level, the choice for the location of points for the generation of floor response spectra (FRS) is critical. One rational approach is to generate FRS at the CG of each level and to use those for the design of components and systems supported at that level. It is also essential to select appropriate points on the floor critical for the equipment design including supports.

FLOOR RESPONSE SPECTRA GENERATION

Generally, time-history methods are used for generating FRS from floor time histories because of their simplicity and reliability. For a conservative design of SSCs, a direct method, which is simple and less time consuming, may be adopted.

1. Direct Method: Time History Analysis

a) For the design basis ground motion, time history analysis is performed by using a mathematical model of the structure, which could be a beam or 3-D FE model, and floor time histories are generated.
b) FRS are generated by using the floor time histories. While generating FRS, the spectrum ordinates are computed at sufficiently small intervals to produce accurate response spectra including significant peaks normally expected at the natural frequencies of the structure. One acceptable interval of frequencies is listed in Table 6, which is as per ASCE 4-1998 standard (ASCE, 2000). Figure 13 shows the FRS at various levels generated for an AHWR building.

Table 6: Frequency Steps for FRS Generation

Frequency Range (Hz)	Increment (Hz)
0.5–3.0	0.10
3.0–3.6	0.15
3.6–5.0	0.20
5.0–8.0	0.25
8.0–15.0	0.50
15.0–18.0	1.0
18.0–22.0	2.0
22.0–34.0	3.0

2. Stochastic Analysis

The various steps involved in a stochastic method are given below:

a) The design basis ground motion, denoted by design basis Power Spectral Density Function (PSDF), is generated.
b) A mathematical model of the structure is generated. The model could be a beam or 3-D FEM model.
c) The floor PSDF is generated from the design basis PSDF by using structural analysis.
d) FRS are now generated from the floor PSDF at the frequency interval explained above.

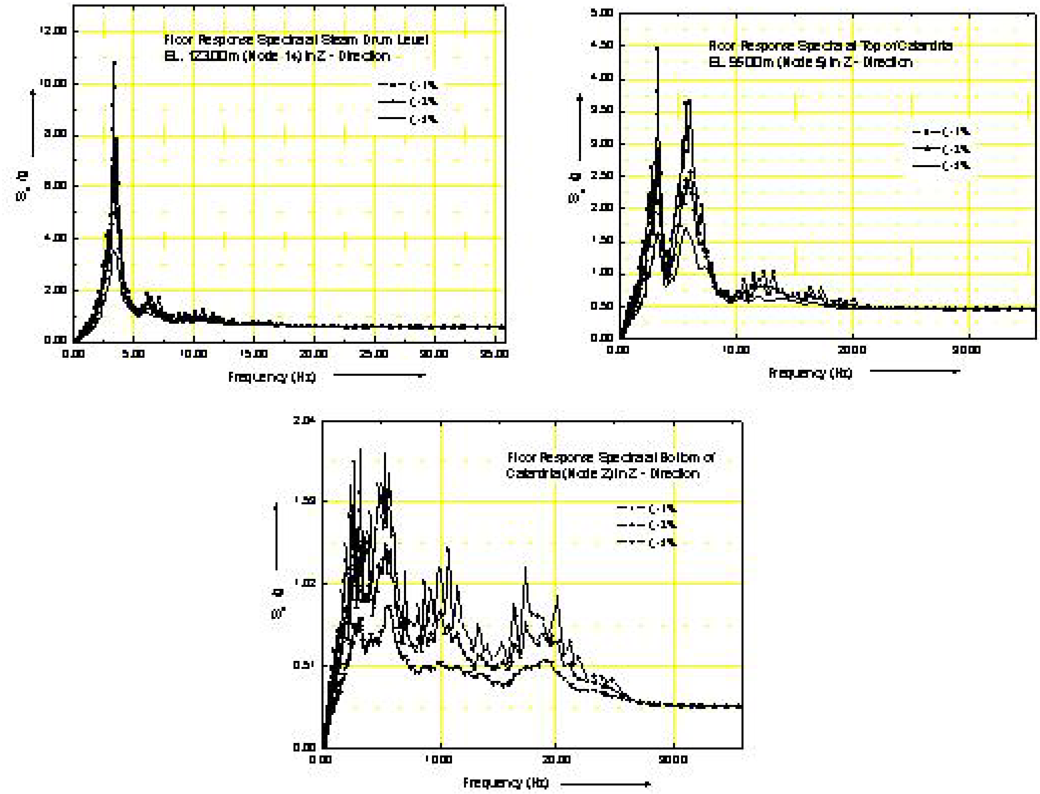

Fig. 13 Floor response spectra at various floor levels of the AHWR building

3. Simplified Analysis

The various steps involved in a simplified analysis are given below:

(a) The design basis ground motion, denoted by design basis response spectrum as shown in Figure 14(b) and compatible time history as shown in Figure 14(c), is generated for the given structural damping.

(b) A mathematical model of the structure as shown in Figure 14(a) is generated. This could be a beam or 3-D FEM model.

(c) FRS are generated based on the procedure outlined below:

$$S_{Ei} = \frac{1}{\sqrt{\left[1-\left(\frac{\omega_A}{\omega_{Bi}}\right)^2\right]^2 + 4\left(h_A + h_{Bi}\right)^2\left(\frac{\omega_A}{\omega_{Bi}}\right)^2}} \sqrt{\left[\left(\frac{\omega_A}{\omega_{Bi}}\right)^2 S\left(\omega_{Bi}, h_{Bi}\right)\right]^2 + S^2\left(\omega_A, h_A\right)} \tag{11}$$

$$S_B = \sqrt{\sum_i \left({}_\beta U_i S_{Ei}\right)^2} \tag{12}$$

where

S_E is the floor response spectrum taking into account every evaluated mode of the structure;

${}_\beta U_i$ is the ith-mode excitation function value of the floor and is equal to the product of modal participation factor and floor mode shape in the ith mode;

S_{Ei} is the maximum value of the absolute acceleration response of the system and components under the ith-mode acceleration of the structure;

h_A is the damping factor of the systems and components;

T_A is the natural period of the system and components;

h_{Bi} is the damping factor of the structure;

T_{Bi} is the natural period of the structure;

$S(T_{Bi}, h_{Bi})$ is the standard design ground spectrum corresponding to T_{Bi} and h_{Bi} of the structure; and
$S(T_A, h_A)$ is the standard design ground spectrum corresponding to T_A and h_A of the structure.

It may be noted that the mass m_A of the system and components needs to be sufficiently smaller than the mass m_{Bi} of the structure.

At least 10% broadening of the floor response spectrum needs to be taken into account to cope up with the uncertainty in the frequency analysis of SSCs.

By using the above procedure, FRS at the top of the building are generated and compared with the time history analysis results as shown in Figure 14(d). It may be seen that the spectra generated by using the simplified method are conservative compared to those generated by using the time history analysis.

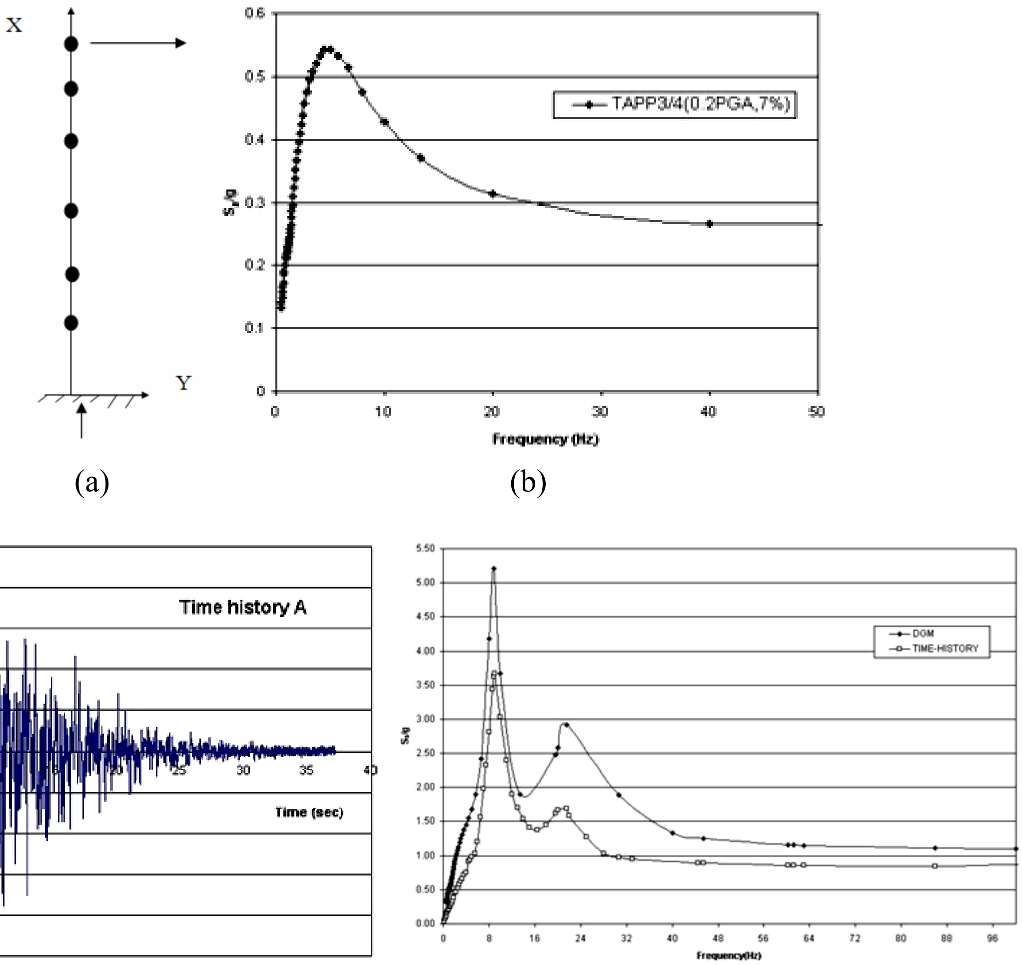

Fig. 14 (a) Beam model of typical cantilever structure; (b) Typical design spectrum (0.2*g* PGA, 7% damping); (c) Time history compatible with the given spectra; (d) FRS at the top of the building

SEISMIC RE-QUALIFICATION OF EXISTING NPP STRUCTURES, EQUIPMENT AND PIPING SYSTEMS

The objective of the seismic review of an existing nuclear safety-related facility is its evaluation against the perceived seismic hazard by using the current design practice. The methodology of seismic design of structures, equipment and piping systems has evolved over a number of years, and several important nuclear safety-related facilities were designed and built according to the standards prevailing at the time of their construction. These facilities may not satisfy the requirements which are related to the current design criteria, as explained above, for NPP systems for their protection against the effects of seismic hazard. Therefore, it becomes necessary to reassess the capability of the older NPP systems to withstand the effects of earthquake loads in line with the present statutory requirements.

Broadly, the seismic review methodology has four steps, namely,

(i) determination of an earthquake level for the seismic re-assessment, which is generally higher than the one for which the facility had been originally designed;
(ii) identification of the systems for which the seismic re-assessment is to be carried out;
(iii) assessment of the seismic capacity of the NPP systems with respect to the derived higher earthquake load as per the current design practice; and
(iv) wherever necessary, upgradation of the structures by using the information obtained from the seismic re-qualification.

The seismic capacity of an NPP system is the ground acceleration up to which the system would have the ability to sustain its effects and would continue to perform its intended functions. The seismic capacity can be assessed by detailed analysis and design that are backed by experience (INSAG, 1995). However, the re-qualification methodology for systems involves

(i) analyzing the systems for the derived higher level of ground motion and determining design forces, and
(ii) re-evaluating the design forces, while considering the inelastic energy absorption characteristics of the systems by adopting suitable ductility factor and a higher value of damping (as in Table 7), for the re-qualification of the systems in the existing plants (INSAG, 1995).

Table 7: Damping Values (as Percentages of Critical Damping) for Seismic Re-qualification

System	Damping
Reinforced Concrete Structures	10
Steel Frame Structures	15
Welded Assemblies	7
Bolted and Riveted Assemblies	15
Cable Trays	10
Heat Exchangers, Pumps and Tanks	7
Piping	5

Nearly all the systems used in NPPs and made of ductile material exhibit some ductility before failure. The easiest way to account for the inelastic absorption capability in civil structures is to multiply the computed seismic stresses by a reduction factor of 0.8. However, sometimes a detailed non-linear analysis is performed to justify lower values. In the case of piping, the allowable stress value of 4.5 S_m for earthquake loads is permitted. The S_m value is taken as the minimum of two-third of yield stress or one-third of ultimate stress. The plant walk-down criteria for evaluating seismic margin are also used. While re-evaluating stress in the pipe support, the allowable stress for structural steel may be considered as 1.3 times the yield stress.

By using the above-outlined procedure, Madras atomic power plant and Dhruva research reactor have been requalified for the present seismic design requirements.

STANDARDIZATION AND RETROFITTING

One of the contributors in increasing the cost of an NPP is seismic design. A cost-effective seismic design of NPP is possible, if the seismic design is standardized. This can be achieved by using passive seismic response control devices, such as isolators (Varma el al., 2002), energy absorbers of elasto-plastic type, lead-extrusion type (Parulekar et al., 2004), or friction type (Reddy et al., 1999). A substantial progress has been made in the design and testing of isolators, elasto-plastic dampers and lead-extrusion dampers, shown respectively in Figures 15, 16 and 17. These devices can also be used for the purpose of retrofitting of existing NPP systems. An analysis of NPP systems supported on the above devices by using direct and linearization techniques (Reddy et al., 1999) can be performed.

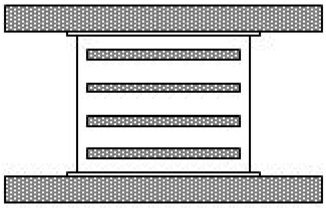

Fig. 15 Laminated rubber bearing (test model)

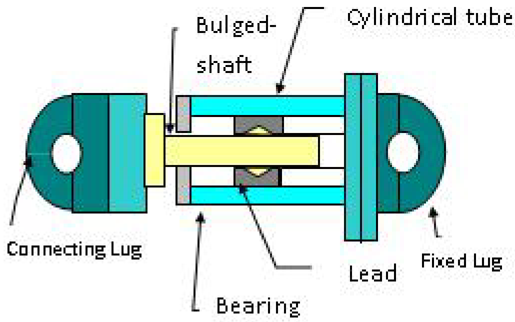

Fig. 16 Lead extrusion damper

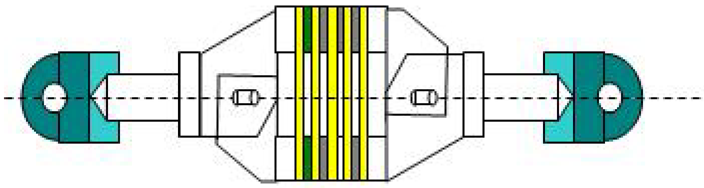

Fig. 17 Elasto-plastic damper (EPD)

ACKNOWLEDGEMENTS

The author acknowledges the contributions of Mr. R. Reddy, Mr. K.K. Vaze, Mr. H.S. Kushwaha of Bhabha Atomic Research Centre, Mumbai and Mr. H.A. Mapari of Tata Consulting Engineers Limited, Mumbai in the preparation of this paper. The author is grateful to two organizations—Bhabha Atomic Research Centre, Mumbai and Tata Consulting Engineers Limited, for providing the environment to carry out such extensive design-oriented research work during the engineering of various projects.

REFERENCES

1. Arya, S.C., O'Neill, M.W. and Pincus, G. (1979). "Design of Structures and Foundations for Vibrating Machines", Gulf Publishing Company, Houston, U.S.A.
2. ASCE (2000). "ASCE 4-1998: Seismic Analysis of Safety-Related Nuclear Structures and Commentary", ASCE Standard, American Society of Civil Engineers, Reston, U.S.A.
3. Bathe, K.-J. and Wilson, E.L. (1976). "Numerical Methods in Finite Element Analysis", Prentice-Hall of India Private Limited, New Delhi.
4. BIS (1975). "IS 1893-1975: Indian Standard Criteria for Earthquake Resistant Design of Structures", Bureau of Indian Standards, New Delhi.
5. BIS (2002). "IS 1893-2002 (Part 1): Indian Standard Criteria for Earthquake Resistant Design of Structures, Part 1—General Provisions and Buildings", Bureau of Indian Standards, New Delhi.
6. INSAG (1995). "A Common Basis for Judging the Safety of Nuclear Power Plants Built to Earlier Standards", Report INSAG-8, International Atomic Energy Agency, Vienna, Austria.
7. Parulekar, Y.M., Reddy, G.R., Vaze, K.K. and Kushwaha, H.S. (2004). "Lead Extrusion Dampers for Reducing Seismic Response of Coolant Channel Assembly", Nuclear Engineering and Design, Vol. 227, No. 2, pp. 175–183.
8. Reddy, G.R., Vaze, K.K., Kushwaha, H.S., Tandale, J.V., Subramanian, K.V. and Kelkar, S.P. (1994). "Procedure of Applying Decoupling Criteria for a Complex Primary and Secondary System", Proceedings of the 1994 Pressure Vessels & Piping Conference, Minneapolis, Vol. 1, pp. 129–139.
9. Reddy, G.R., Kushwaha, H.S., Mahajan, S.C., Kelkar, S.P. and Karandikar, G.V. (1996). "Development of 3-D Beam Model for Seismic Analysis of 500 MWe Reactor Building", Report BARC/1996/I/004, Bhabha Atomic Research Centre, Mumbai.

10. Reddy, G.R., Suzuki, K. and Mahajan, S.C. (1997). "Beam Model for Seismic Analysis of Complex Shear Wall Structure Based on the Strain Energy Equivalence", JSME International Journal Series C, Vol. 40, No. 4, pp. 652–664.
11. Reddy, G.R., Kushwaha, H.S., Mahajan, S.C. and Suzuki, K. (1998). "Decoupling Criteria for Multi-Connected Equipment", Journal of Pressure Vessel Technology, ASME, Vol. 120, No. 1, pp. 93–98.
12. Reddy, G.R., Suzuki, K., Watanabe, T. and Mahajan, S.C. (1999). "Linearization Techniques for Seismic Analysis of Piping System on Friction Support", Journal of Pressure Vessel Technology, ASME, Vol. 121, No. 1, pp. 103–108.
13. USNRC (1976). "Combining Modal Responses and Spatial Components in Seismic Response Analysis", Regulatory Guide 1.92 (Revision 1), U.S. Nuclear Regulatory Commission, Washington, D.C., U.S.A.
14. USNRC (1989). "Section 3.7.2 (Revision 2): Seismic System Analysis" in "Standard Review Plan for the Review of Safety Analysis Reports for Nuclear Power Plants", Report NUREG-0800, U.S. Nuclear Regulatory Commission, Washington, D.C., U.S.A.
15. USNRC (2006). "Combining Modal Responses and Spatial Components in Seismic Response Analysis", Regulatory Guide 1.92 (Revision 2), U.S. Nuclear Regulatory Commission, Washington, D.C., U.S.A.
16. USNRC (2007a). "A Performance-Based Approach to Define the Site-Specific Earthquake Ground Motion", Regulatory Guide 1.208, U.S. Nuclear Regulatory Commission, Washington, D.C., U.S.A.
17. USNRC (2007b). "Damping Values for Seismic Design of Nuclear Power Plants", Regulatory Guide 1.61 (Revision 1), U.S. Nuclear Regulatory Commission, Washington, D.C., U.S.A.
18. Varma, V., Reddy, G.R., Vaze, K.K. and Kushwaha, H.S. (2002). "Experimental and Analytical Study of Laminated Rubber Bearings and Its Application to PHWR Building", Journal of Structural Engineering, SERC, Vol. 28, No. 4, pp. 199–204.